Delft University of Technology

Recent Advances in Ferroelectret Fabrication, Performance Optimization, and Applications

Wang, Ningzhen; Zhang, He; Qiu, Xunlin; Gerhard, Reimund; van Turnhout, Jan; Cressotti, Jason; Zhao, Dong; Tang, Liang; Cao, Yang

Important note
To cite this publication, please use the final published version (if applicable).
Please check the document version above.

Recent Advances in Ferroelectret Fabrication, Performance Optimization, and Applications

Ningzhen Wang, He Zhang, Xunlin Qiu, Reimund Gerhard, Jan van Turnhout, Jason Cressotti, Dong Zhao,* Liang Tang,* and Yang Cao*

The growing demand for wearable devices has sparked a significant interest in ferroelectret films. They possess flexibility and exceptional piezoelectric properties due to strong macroscopic dipoles formed by charges trapped at the interface of their internal cavities. This review of ferroelectrets focuses on the latest progress in fabrication techniques for high temperature resistant ferroelectrets with regular and engineered cavities, strategies for optimizing their piezoelectric performance, and novel applications. The charging mechanisms of bipolar and unipolar ferroelectrets with closed and open-cavity structures are explained first. Next, the preparation and piezoelectric behavior of ferroelectret films with closed, open, and regular cavity structures using various materials are discussed. Three widely used models for predicting the piezoelectric coefficients (d_{33}) are outlined. Methods for enhancing the piezoelectric performance such as optimized cavity design, utilization of fabric electrodes, injection of additional ions, application of DC bias voltage, and synergy of foam structure and ferroelectric effect are illustrated. A variety of applications of ferroelectret films in acoustic devices, wearable monitors, pressure sensors, and energy harvesters are presented. Finally, the future development trends of ferroelectrets toward fabrication and performance optimization are summarized along with its potential for integration with intelligent systems and large-scale preparation.

1. Introduction

With the emergence of Internet of Things and Body Area Networks,[1–3] the demand for noninvasive health monitoring devices that continuously track users' physical conditions in fields like chronic disease treatment,[4–6] sports training, and construction work is growing steadily.[7–9] This has prompted an upswing in research into flexible and biofriendly piezoelectric materials.[10–13]

Traditional piezoelectric materials like piezoelectric ceramics known for their high piezoelectric coefficients and low manufacturing costs,[14] are widely applied in resonators and sensors that must operate at high-temperatures.[15–18] Lead zirconate titanate with a perovskite structure, represented by Pb(Zr,Ti)O$_3$ and abbreviated as PZT, has a d_{33} of 460 pC N^{-1} even at 400 °C.[19] As shown in the lattice model of **Figure 1a**,[20] the displacement of positive and negative ions in the unit cell by a mechanical stress will create dipoles. However, ceramics are typically brittle and heavy.[21] Hence, for applications that require flexibility or skin contact piezoelectric ceramic nanoparticles are often embedded in a polymer matrix.[22–25] In recent years, Bowen and co-workers[26–28] were able to increase the output of piezoelectric ceramic transducers by introducing microscopic and macroscopic pores. These pores also augment the piezocatalysis of ferroelectric ceramics by increasing the effective diffusion coefficient.[26] In order to meet the demands of both output power and flexibility in wearable devices, polymers were blended with porous piezoelectric ceramic arrays.[27]

N. Wang, H. Zhang, D. Zhao, L. Tang
School of Technology
Beijing Forestry University
Beijing 100083, China
E-mail: Zhaodong68@bjfu.edu.cn; happyliang@bjfu.edu.cn
X. Qiu
Shanghai Key Laboratory of Intelligent Sensing and Detection Technology
School of Mechanical and Power Engineering
East China University of Science and Technology
Shanghai 200237, China

R. Gerhard
Institute of Physics and Astronomy
Faculty of Science
University of Potsdam
14476 Potsdam-Golm, Germany
J. van Turnhout
Department of Materials Science and Engineering
Delft University of Technology
Delft 2628 CD, The Netherlands
J. Cressotti, Y. Cao
Electrical Insulation Research Center
Institute of Materials Science
University of Connecticut
Storrs, CT 06269, USA
E-mail: yang.cao@uconn.edu

ADVANCED
SCIENCE NEWS
www.advancedsciencenews.com

**ADVANCED
MATERIALS**
www.advmat.de
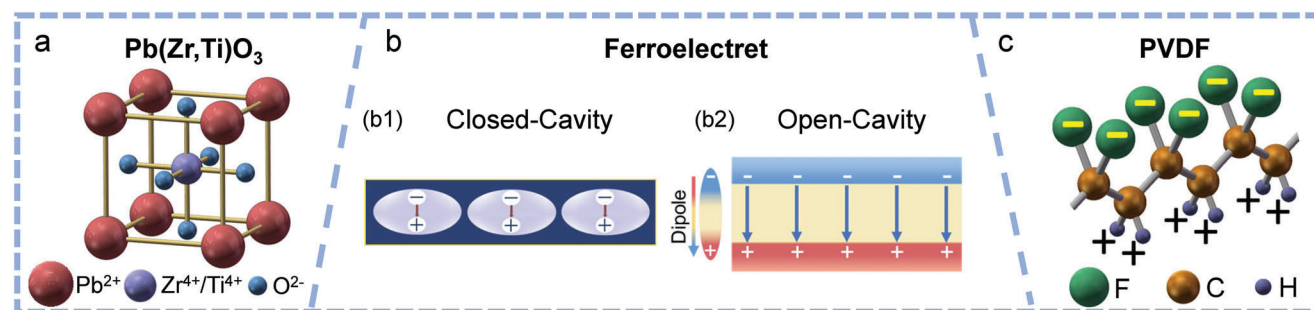
Figure 1. a) Stereoscopic drawing of tetragonal phase PZT. b) Macroscopic polarization of ferroelectret with b1) closed and b2) open-cavity structure. c) Representation of the polar molecule structure in piezoelectric PVDF film.

In the mid-20th century, fluorinated polymer polyvinylidene difluoride (PVDF) was discovered to be piezoelectric due to the dipole moments in its crystalline β-phase molecules (β-PVDF) (Figure 1c).[29] However, its piezoelectric coefficient was often less than 30 pC N^{-1}.[30] This initiated worldwide efforts to elevate its piezoelectric properties and explore piezoelectricity in other flexible polymeric materials.[31–36]

In the late 20th century, Kirjavainen et al.[37,38] uncovered the piezoelectricity of highly charged cellular polypropylene (PP) films, later coined as ferroelectrets.[23,39] The charging mechanism of ferroelectrets differs considerably from the cooperative molecular alignment in PVDF. It is achieved, usually in ambient air, by ionizing gas molecules inside the closed cavities using a strong electric field.[40,41] The separated positive and negative ions caused by dielectric barrier discharges (DBDs) give rise to macroscopic dipoles that are capable of producing a strong internal permanent electric field (Figure 1b1).[42] Moreover, the charges are trapped on the internal surfaces of the cavities, and are therefore shielded to a large extent from the ambient humidity for ferroelectrets with closed cavities. This renders such ferroelectrets, made from a nonpolar polymer, less prone to a loss in sensitivity under moist environments. For example, the piezoelectric activity of cellular PP ferroelectrets is virtually not affected by humidity during prolonged storage in a humid atmosphere or immersion in distilled water.[43–45]

Ever since, ferroelectrets have evolved from many other polymeric films, like polyethylene (PE),[46,47] polyethylene terephthalate (PET),[48,49] polyethylene naphthalate (PEN),[50,51] polytetrafluoroethylene (PTFE),[52–54] fluorinated ethylene propylene copolymer (FEP),[55,56] polylactic acid (PLA),[57,58] cycloolefin polymers (COP) and copolymers (COC),[59,60] and others. Kacprzyk et al.[61–63] explored piezoelectric soft-hard layered systems, such as PP–polystyrene (PS), wherein charges are stored at the interfaces by the Maxwell–Wagner effect. Innovative sandwich-structured ferroelectrets were devised to overcome difficulties in forming cavities in high-temperature resistant polymers.[55] Heat resistant ferroelectrets were made by placing a layer of expanded PTFE (ePTFE) between two layers of FEP films forming an FEP–ePTFE–FEP trilayer structure (Figure 1b2),[64] or by bonding an FEP film with laser-processed pores between two solid FEP films, etc.[65] These novel layered ferroelectret films made from different materials exhibit a variety of mechanical properties, piezoelectric characteristics, and resonance frequency ranges. A challenge posed to ferroelectrets

crafted from fluorinated polymers is that their synthesis requires per- and polyfluorinated alkyl substances, also known as "forever chemicals."[66] Despite this obstacle, many efforts have been devoted on refining the preparation process, improving the piezoelectric performance, and expanding the applications of ferroelectrets made from fluorinated polymers.[43,67,68]

Previous reviews have covered several aspects of ferroelectrets. Zhang et al.[69] reviewed their manufacturing processes, modeling approaches and applications as energy harvesters, focusing in particular on modeling their response to dynamic mechanical loads. Mo et al.[70] critically reviewed the fabrication of ferroelectret nanogenerators (FENGs) and their applications in wearable devices. Zhang et al.[71] summarized the use of ferroelectret films as energy harvesters for collecting low-frequency vibrations and acoustic energy. Li et al.[72] provided an overview of electromechanical physiological signals monitoring using nanogenerators (NGs), wherein ferroelectrets being flexible may play an eminent role. Ansari and Somdee[73] reviewed various preparation methods of piezoelectric nanogenerators (PENGs) using ferroelectrets, with a focus on their energy conversion capabilities. Qiu wrote an overview about the methods for fabrication and polarization of polymer electrets and ferroelectrets, and discussed various routes to enhance the performance of ferroelectrets.[74] He and his colleagues also reviewed new charging methods with high efficiency and presented several illustrative applications.[75,76] Some scholars reviewed forefront applications of ferroelectrets in the biomedical field.[77,78] To bridge the gap toward applications under harsh conditions, this review covers recent advances in fabrication techniques, performance improvement, and new applications of high temperature resistant ferroelectrets, with key topics regarding the fabrication of regular microcavities using additive manufacturing, novel methods for performance enhancement of high temperature resistant ferroelectrets, and their trendy applications in biological equipment.

The review categorizes the manufacturing processes of ferroelectrets based on their cavity structures, followed by a comprehensive analysis of charging methods and a presentation of current approaches of performance enhancement. Section 2 discusses the principles of the charging processes of ferroelectrets with different cavity structures. Section 3 describes for different cavity structures, the fabrication of ferroelectrets from various polymeric materials. Section 4 reviews the models for estimating the d_{33} coefficient, and it further summarizes various methods to augment the piezoelectric performance. Attempts are made
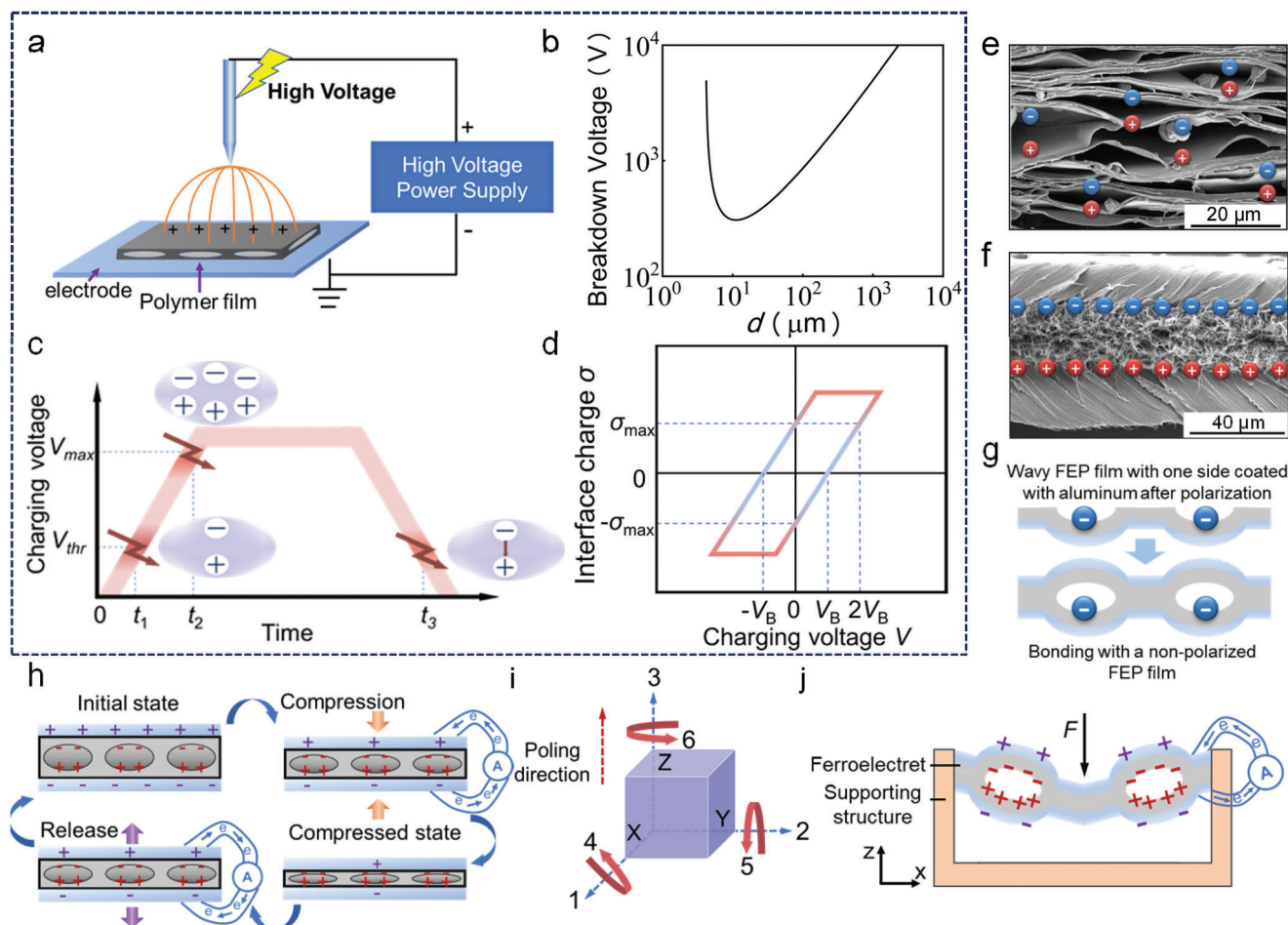
Figure 2. Polarization process, charge distribution inside cavities after polarization and basics of piezoelectric effect. a) Set up of corona charging. Reproduced with permission.[64] Copyright 2021, Wiley-VCH GmbH. b) Paschen breakdown curve. c) Schematic charge profiles inside a cavity during the variation of the applied voltage with time. Adapted with permission.[83] Copyright 2007, AIP Publishing. d) Curve depicting the change in surface charge versus voltage during the polarization. Reproduced with permission.[104] Copyright 2011, IEEE. Illustration of the charge distribution in e) closed-cavity and f) open-cavity ferroelectret films after polarization. g) Polarization of an unipolar ferroelectret film. Reproduced with permission.[94] Copyright 2018, IEEE. h) Piezoelectric effect of ferroelectret films in the thickness direction. Reproduced with permission.[105] Copyright 2021, IEEE. i) Three axes for defining the direction in piezoelectric materials. Reproduced with permission.[101] Copyright 2018, Wiley-VCH GmbH & Co. KGaA. j) Piezoelectric effect of ferroelectret films under a lateral force. Reproduced with permission.[103] Copyright 2018, Elsevier Ltd.

to employ the d_{33} models to analyze the enhancement mechanisms. Section 5 summarizes up the applications of ferroelectrets in many fields, focusing particularly on recent progress. Section 6 concludes the review with proposed directions for the future development of ferroelectret films in terms of fabrication, performance enhancement, and applications.

2. Piezoelectric Mechanism of Ferroelectrets

2.1. Charging Process

2.1.1. Bipolar Ferroelectrets Polarization

The piezoelectric effect of closed-cavity piezoelectret films, such as cellular PP films, originates from the bipolar charging that occurs within their cavities. When a high electric field is applied, during direct contact charging or corona charging, the air within

the many cavities ionizes. This leads to positive and negative charges being generated, separated, and trapped, respectively, at the upper and lower surfaces of the cavities, which give rise to a bipolar polarization.[79]

In comparison to contact polarization, corona charging requires a higher voltage. A setup of corona charging is shown in **Figure 2a**. The voided film is placed on a metal electrode opposite the corona needle. To generate a corona discharge around the needle, the applied voltage needs to exceed a threshold, which depends on the sharpness of the needle and the surrounding gas atmosphere.[80] During corona charging, a surface potential is built up, which induces an internal electric field in the cavities that triggers breakdown of the gas inside. The shape and size of the cavities as well as the kind and pressure of the gas inside determine the strength of the breakdown field.[81] In general, the Paschen breakdown voltage V_b of a cavity exhibits a U-shaped dependence on pd, where p is the gas pressure and d the height of

the cavity. The Paschen breakdown curve in Figure 2b shows the relation between breakdown voltage and cavity height for air at standard atmospheric pressure. For atmospheric air, cavities with a height of around 10 µm are most prone to internal discharge at a low breakdown voltage. On the left branch of the Paschen curve, V_b increases sharply with decreasing cavity height. Because of the limited number of gas molecules present in the cavity, quite a high voltage is needed to supply enough energy to the electrons to trigger breakdown. Conversely, on the right branch of the Paschen curve, V_b increases more or less linearly with d, because the breakdown field remains almost unchanged in this range. The cavity size in the thickness direction of films for charging is typically between 8 and 100 µm.[74,82]

Qiu et al.[83,84] analyzed the DBD process in closed cavities during charging. As illustrated in Figure 2c, with an increasing voltage, air in the cavities starts to ionize at the threshold voltage (V_{thr}) (point 1) and this continues until most of the air pockets have experienced DBDs. The resulting bipolar charges are trapped at the internal surfaces, creating an electric field opposing the applied field and gradually reducing the internal discharges. As the voltage is increased further, the air in the cavities undergoes DBDs anew (point 2). When the voltage decreases, at point 3, "back discharges" begin to emerge within the cavities.[85] These reverse discharges persist until the voltage reaches zero, signifying completion of the charging process.[83] The voltage at which discharges occurs will alter with the air pressure. It may decrease first and then increase, depending on the height of cavities.[86,87] Figure 2e depicts schematically the charge profile within cellular PP ferroelectret film after charging, with bipolar charges trapped at the surfaces of the closed cavities forming strong macrodipoles.

The DBD process for an FEP–ePTFE–FEP structure with open pores is similar to that of cellular PP film with the two solid FEP layers on the upper and lower side serving as charge-blocking walls.[88] The three-layered structure resembles a film with one single macroscopic cavity formed by the porous ePTFE film that is enclosed by the two FEP layers. With an increase of the applied voltage, ambient air within the ePTFE fiber layers will ionize by DBDs. Throughout this process, separated positive and negative charges are, for a large part, trapped at the FEP/ePTFE interfaces. Upon removal of the applied voltage, the positive and negative charges captured constitute the final macroscopic polarization (Figure 2f).[80,89,90] Due to the interconnected pores inside the ePTFE layer, ionization will occur through adjacent pores. The breakdown voltage will therefore not increase much even when the pore size becomes less than 8 µm.[91] Zhang et al.[92] and Zhukov et al.[80] demonstrated the dynamic relation between the effective polarization of ferroelectrets and the charging voltage (Figure 2d). When the charging voltage exceeds twice the breakdown voltage (V_B), the residual internal space charge will reach its maximum (σ_{max}) after the external voltage is removed.

2.1.2. Unipolar Ferroelectret Polarization

Unipolar ferroelectrets are appealing, because of their superior charge stability.[93–96] A material that carries unipolar charges shall not easily lose its charges by detrapping or Ohmic conduction. Both direct contact charging and corona charging can deposit preferentially unipolar charges on a film surface, usually negative, in view of their excellent stability in fluorocarbon-based polymers.[97] Unipolar polarization is achieved in sandwich structures with open-cavity structures or regular single-layer tubular pores inside, because unipolar charges can only be filled in the open porous structure by unipolar polarization, and then it needs be encapsulated by an upper film, whereas closed-cavity structures cannot meet the conditions for unipolar polarization. Typically, a thin layer of aluminum is first coated as electrode on the convex surface of an FEP film with a wavy structure. Then a needle carrying a voltage of about −10 kV is positioned close to the concave side of the FEP film to deposit negative charges. The fabrication process of the curved FEP film and its potential applications will be worked out in Section 3.3. Subsequently, an uncharged FEP film with a complementary wavy structure and aluminum electrode is bonded to the charged wavy FEP film. This creates unipolar FEP ferroelectrets with an open cavity tunnel structure, as depicted in Figure 2g.[94] Preferably, negative charges are trapped in the inner cavities, because this results in a highly stable unipolar ferroelectret that can be used for a variety of applications, where a long-lasting polarization is crucial. It should be noted, however, that unipolar ferroelectrets will generate less piezoelectricity than bipolar ones, because their piezoelectricity can only be derived from nonaffine deformations. This disadvantage can be overcome by layering a unipolar open-pore electret carrying a positive charge on top of a negatively charged one. Such an assembly will undoubtedly show a high piezoelectricity with also long-term stability.

2.2. Piezoelectric Properties

After applying aluminum or other electrodes to both sides of a ferroelectret film, positive and negative charges are induced on the electrodes by the charges stored internally in their cavities. This creates an electric field along the thickness direction. When pressure is applied, the dipole moment in the ferroelectret film will change, leading to a corresponding change in the induced charges on the electrodes. This phenomenon, known as piezoelectric effect, generates a current in the external circuit.[98] If we consider a cellular PP ferroelectret film as an example, as shown in Figure 2h, the dipole moment of the macroscopic dipoles (i.e., the charged cavities) decreases when pressed. At the same time the cavities will impede any drift of charges along the thickness direction.[99] Consequently, the amount of charge accumulated on the electrodes alters, resulting in a measurable current in the sensing circuit.[39,100] Releasing the pressure allows the dipole moment of macroscopic dipoles to revert, leading to an increase of the charge induced on the electrodes thereby generating a current in the opposite direction. This reversible process enables ferroelectret films to convert mechanical energy into electrical energy. Similarly, applying an oscillating voltage to the electrodes causes ferroelectrets to vibrate, thereby converting electrical energy into mechanical energy. Due to this reciprocal mechanism, ferroelectret films find numerous applications in sensors, nanogenerators, actuators, acoustic devices, and many other areas.

To quantify the piezoelectric performance of ferroelectric films, piezoelectric coefficients are employed, analogous to other piezoelectric materials. In the coordinate system of Figure 2i,

**ADVANCED
SCIENCE NEWS**

www.advancedsciencenews.com

**ADVANCED
MATERIALS**

www.advmat.de

the direction-3 always coincides with the polarization direction. When a force is applied in this direction (which points in the thickness direction), the piezoelectric coefficient is denoted by d_{33}[101]

$$d_{33} = \left(\frac{\partial D_3}{\partial T_3} \right)_E \quad (1)$$

where D_3 and T_3 are the electric displacement and the mechanical stress in the direction-3. This is also the direction, along which the piezoelectric effect of the ferroelectret films is the most prominent. Ferroelectret films may also feature transverse piezoelectricity. For instance, tubular cavity FEP ferroelectret film, which contains tubular open-pores shows noteworthy piezoelectric effects when subjected to a lateral (direction-1) stress (Figure 2j).[102] In such cases, piezoelectric coefficients labeled d_{31} or g_{31}, are used to represent the transverse piezoelectric effect.[103]

3. Fabrication of Ferroelectrets with Different Cavity Structures

3.1. Closed-Cavity Structures

In the domain of ferroelectrets with closed-cavities, pioneer work was undertaken in Finland in the 1990s. It led to a commercial product called EMFi-PP made by physical foaming.[106] This cellular PP became the workhorse of ferroelectret research due to its efficient charge storage, excellent fatigue resistance, and low costs.[107] Various other polymers with high-grade charge stability are amenable to physical foaming. They also can be transformed into ferroelectrets by charging, after which they can be applied in flexible piezoelectric sensors, nanogenerators, acoustic devices, etc. Traditionally, cavities within the polymer films are formed by two techniques: biaxial stretching of filler-loaded polymers and gas-assisted extrusion foaming.[108,109] Polymers with lens-shaped pores that have a width-to-height ratio of ≈6.6 and a transverse dimension of ≈30 μm can be polarized at a lower voltage. This will be discussed in Section 4.2.1.[110]

In the biaxial stretching process of filler-loaded polymers, e.g., polypropylene (**Figure 3a1**), PP powder, stiff mineral particles such as $CaCO_3$, and other additives are mixed thoroughly and then extruded and molded into a film. This film is next stretched in two directions. During this process high stresses build up around the rigid $CaCO_3$ particles, which lead to localized fracture of the stretched PP film in the vicinity of the $CaCO_3$ particles. As a result, tiny lens-shaped cavities emerge within the film, whose dimensions can be adjusted by varying the stretching force (Figure 3a2). Nagō et al.[111,112] demonstrated that the smaller the size of the $CaCO_3$ particles, the larger the effective porosity and the smaller the cavity diameter become. Gilbert-Tremblay et al.[113] used 12 μm $CaCO_3$ particles and obtained a cellular PP film with a relative density of 0.8. They found that the $CaCO_3$ particles need to have a minimum diameter of 3 μm to initiate and propagate cracks effectively during film stretching. In another approach, Behrendt et al.[114] filled isotactic polypropylene (i-PP) with NA11 (2,2′-methylene-bis-(4,6-di-tert-butylphenyl)-phosphate) particles and hollow glass spheres

and then stretched the material to obtain cellular i-PP films (Figure 3a3). They observed that cellular i-PP films prepared with 10 wt% NA11 and mixed with glass spheres of an average diameter of 30 μm preserve outstanding charge storage. They obtained a d_{33} value of around 179 pC N^{-1} after charging. The manufacturing process and piezoelectric performance of some typical ferroelectrets mentioned in Section 3.1 and 3.2 are highlighted and summarized in **Table 1**.

Biaxial stretching was also used to prepare other ferroelectrets, such as polyetherimide (PEI) and COC.[59,115] Behrendt[115] performed stretching of PEI mixed with hollow glass spheres. Saarimäki et al.[59] prepared cellular COC films, which retained their piezoelectric properties at 110 °C (Figure 3a4). Often, cavities will open spontaneously during the stretching of polymers that contain tiny rigid particles. Their cavities are too flat for efficient DBD charging, because electrons cannot be accelerated sufficiently enough to ionize the gas molecules.[23] In addition, flat cavities make films rather stiff, which results in a low electromechanical response.

The size of the internal cavities can be adjusted, with expansion or inflation by means of high-pressure gas in combination with a thermal treatment.[116–118] For this adjustment, polymer foam is placed inside a chamber into which high-pressure gas is fed. With time, the gas molecules diffuse into the cavities until the pressure within the cavities equalizes that in the chamber. The foam is then inflated by a sudden release of the high gas pressure. After this, the inflated foam structure is stabilized by a heat treatment at elevated temperatures during or right after the pressure release (Figure 3a5). It was noticed that higher heating temperatures cause a higher porosity. PP films processed through this method attained a d_{33} value of 590 pC N^{-1}; however, this method has limitations, as it requires polymers with a relatively low melting point to mix well with inorganic fillers. This may end in a nonuniform cavity-size distribution.

An alternative foaming viz. foam extrusion was therefore invoked to fabricate cellular polymeric ferroelectrets. In gas-assisted extrusion, the most common approach is foaming with a supercritical (sc) fluid (such as sc-CO_2 and sc-N_2), sometimes followed by a biaxial stretching and gas-diffusion inflation for further optimization of the foam structure (Figure 3b1).[119] Mohebbi et al.[110,120] investigated the impact of the heat treatment parameters and applied supercritical N_2 (scN_2) pressure to control the cavity geometry. By employing a pressure treatment with gradually increased temperature, lens-shaped pores with a width-to-height ratio of 6.6 were obtained. This led to a 45% increment of the piezoelectric d_{33} coefficient to 800 pC N^{-1}, cf. Table 1.

Gas-assisted extrusion foaming is widely employed in the fabrication of porous structures in polymers, like PET,[121] PEN,[50,51] FEP,[55] PE,[46] and PLA.[57,58] Cellular FEP films composed by Voronina et al.[55] using this approach showed a d_{33} of 50 pC N^{-1} after −60 kV corona charging (Figure 3b2). Cellular PET films produced using foam extrusion (Figure 3b3) exhibited a higher thermal stability than cellular PP films, and good performance over a broader resonance frequency range, indicating promising potential for ultrasound application.[121] The cellular PEN films from Fang et al.[50,51] retained 70% of their piezoelectric performance after a 1 h heating at 100 °C (Figure 3b4).

In recent years, ferroelectrets prepared from the popular biodegradable polymer PLA has attracted much attention.[122]

**ADVANCED
SCIENCE NEWS**

www.advancedsciencenews.com

**ADVANCED
MATERIALS**

www.advmat.de
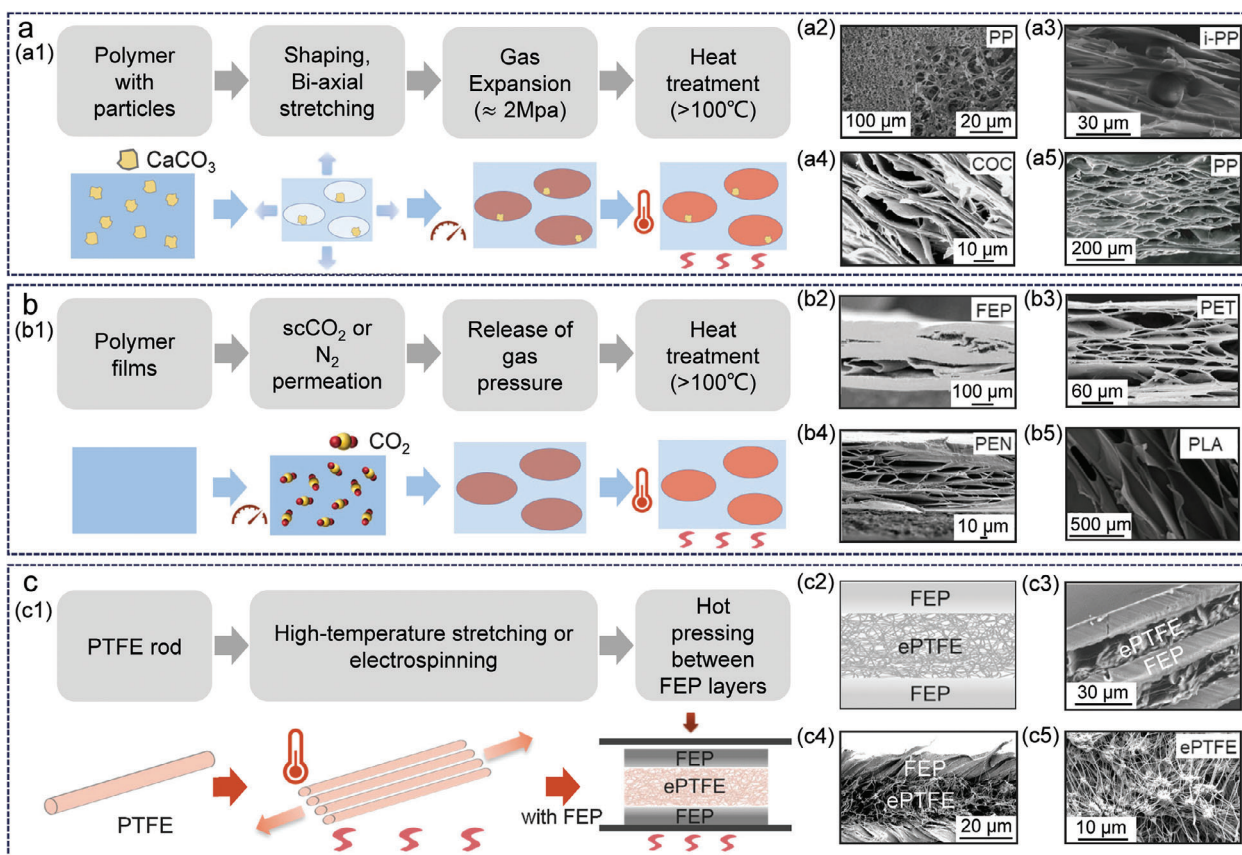
Figure 3. Fabrication methods and cross-sectional scanning electron microscope (SEM) images of porous films. a) Biaxial stretching for films with closed cavities. a1) Diagram of the procedure for biaxial stretching. Longitudinal cross-sectional SEM images of cellular a2) PP. Reproduced with permission.[111] Copyright 1992, John Wiley & Sons. a3) i-PP. Reproduced with permission.[114] Copyright 2006, IEEE. a4) COC. Reproduced with permission.[59] Copyright 2006, IEEE. a5) PP. Reproduced with permission.[117] Copyright 2004, IOP Publishing Ltd. b) Gas-assisted foaming of films with a closed-cavity structure. b1) Diagram of the procedure for foam extrusion. Longitudinal cross-sectional SEM images of cellular b2) FEP. Reproduced with permission.[55] Copyright 2007, Springer. b3) PET. Reproduced with permission.[121] Copyright 2007, Wiley-VCH GmbH & Co. KGaA. b4) PEN. Reproduced with permission.[50] Copyright 2010, IEEE, b5) PLA. Reproduced with permission.[57] Copyright 2020, AIP Publishing. c) Fabrication of films with an open pore structure. c1) Diagram of the fabrication of PTFE and FEP-based sandwich-structured films. c2) Cross-section of the porous sandwich structure. Longitudinal cross-sectional SEM images of c3) laminated film with a five-layer laminate of porous PTFE and FEP. Reproduced with permission.[134] Copyright 2008, AIP Publishing. c4) ferroelectret film of FEP–ePTFE–FEP. Reproduced with permission.[64] Copyright 2021, Wiley-VCH GmbH. c5) SEM image of ePTFE film surface with a pore size of 1 µm. Reproduced with permission.[64] Copyright 2021, Wiley-VCH GmbH.

Zhukov et al.[57] applied physical foaming to PLA, and achieved a high piezoelectric coefficient of 600 pC N^{-1} after brief hot-pressing (Figure 3b5) and polarization. Vadas et al.[58] proposed a more efficient method for generating anisotropic cavities in PLA films, by using a supercritical CO_2 (scCO$_2$)-assisted extrusion with a belt puller. This method produces less waste and is efficient and environmentally friendly.

Besides these two classic methods for closed-cavity production, there are special techniques, such as high-energy electron irradiation to form irradiation crosslinked polypropylene (IXPP).[123,124] This also helps to enhance the piezoelectric performance by adjusting the cell arrangement in ferroelectrets.

3.2. Open-Cavity Structures

The most widely used PP ferroelectret prepared by physical foaming, can operate for continuous use only up to 60 °C.[125]

In the field of wearable electronics, where high-temperature-resistant devices are crucial for prolonged exposure to sunlight, ferroelectrets drafted from PTFE and FEP have attracted much attention owing to their excellent charge stability at elevated temperatures.[54,126–129]

Remke and von Seggern uncovered experimentally the lon-glasting charge storage of PTFE and FEP;[130] however, the dense structure of FEP and PTFE confines any charge storage to the surface.[131] To overcome this limitation, porous PTFE emerged as a solution, despite the challenges of physical forming of optimal cavity structures in high-temperature-resistant materials. Xia et al.[52,99,132] made porous PTFE films with a porosity of ≈50% through biaxial stretching. They concluded that porous PTFE films exhibit the highest charge stability among organic electret materials. This stretched PTFE is referred to as expanded PTFE (ePTFE) in later studies. Additionally, PTFE films with local voids can be prepared using electrospinning. This open-cavity foam is known as fibrous PTFE (f-PTFE). Unfortunately, charges stored

Table 1. Summary of ferroelectret films with various closed or open cavity structures.

	Author	Polymer	Manufacture method	d_{33} [pC N^{-1}]	Output power	Highlights
Biaxial stretching	Behrendt et al. (2006)[114]	i-PP	Stretching with NA11 particles and hollow glass spheres	179	–	The influence of NA11 particles and glass spheres was investigated.
	Saarimäki et al. (2006)[59]	COC/COP	Stretching with mixed mineral fillers and applying N$_2$ inflation. (6 MPa)	15	–	Show good thermal stability up to 110 °C.
	Wegener et al. (2004)[117]	PP	A two-step inflation process (N$_2$ 5 MPa)	590	–	The separation of high-pressure inflation and heat treatment renders the expansion process more flexible.
Gas-assisted physical foaming	Mohebbi et al. (2016)[110]	PP	A two-step inflation (scN$_2$ 5 MPa)	800	–	The piezoelectric d_{33} coefficient increased by 45% through progressive heat treatment.
	Wirges et al. (2007)[121]	PET	A two-step inflation (scCO$_2$ 100 bars)	470	–	Discharge occurs in a sulfur hexafluoride (SF$_6$) atmosphere.
	Fang et al. (2007)[50]	PEN	A two-step inflation (scCO$_2$ 150 bars)	140	–	Higher long-term operating temperature (100 °C)
	Zhukov et al. (2020)[57]	PLA	A two-step inflation (an industrial foaming production line)	600	–	Preliminary study on the piezoelectric properties of the physically foamed biodegradable PLA.
	Vadas et al. (2023)[58]	PLA	A scCO$_2$-assisted extrusion foaming (scCO$_2$ 80–95 bars)	320	–	The processing method was optimized to be simpler and environmentally friendly.
Vacuum treatment	Hu and von Seggern (2006)[53]	FEP–ePTFE–FEP	45 min of vacuum treatment in a brass holder	400–900	–	Sandwich-structured ferroelectret film with excellent piezoelectric performance was prepared using a vacuum method.
Hot pressing	Zhang et al. (2007)[133]	FEP–PTFE–FEP–PTFE–FEP	Hot pressing (10 kPa, 280 °C)	500–2200	–	Higher d_{33} and increased thermal stability compared to traditional PP films.
	Huang et al. (2008)[134]	FEP–PTFE–FEP–PTFE–FEP	Hot pressing (3.3 kPa, 280 °C)	400	–	The charge drift paths were studied at different temperatures.
	Wang et al. (2021)[64]	FEP–ePTFE–FEP	Hot pressing (5 kN, 285 °C)	–	1 µW	The prepared nanogenerator operated stably at 90 °C and performed well 9 months after being polarized.
Bonding	Shi et al. (2018)[137]	FEP–porous polymer	Bonding with double-sided adhesive tape	1000	62.4 µW cm^{-2}	Low-cost, rapidly fabricated, lightweight, and flexible
	Shi and Beeby (2022)[138]	FEP–silk textile	Bonding with double-sided adhesive tape	987	2.26 µW cm^{-2}	The impact of textile properties on the performance of ferroelectret films was investigated.

**ADVANCED
SCIENCE NEWS**

www.advancedsciencenews.com

**ADVANCED
MATERIALS**

www.advmat.de

inside open-porous PTFE films are partially lost when they are metalized on two sides. Due to the interconnected porous structure, metallic particles easily enter voids near the surface and thus destroy part of the trapped charges.[88] To avoid this loss a sandwich structure is usually assembled with a layer of ePTFE placed between two layers of solid FEP films (Figure 3c1).

Hu and von Seggern[53] prepared a sandwich-structured film with open pores using a vacuum-assisted method, as illustrated in Figure 3c2. For a nominal ePTFE porosity of 91%, the d_{33} value remained at 400 pC N^{-1} 5 days after the charging. Zhang et al.[133] hot-pressed multiple layers comprising alternating 12.5 μm thick ePTFE and 12.5 μm thick FEP layers at 280 °C. Their ferroelectret film demonstrated a high thermal stability, with a d_{33} of more than 500 pC N^{-1} after 1-day storage at 90 °C. Huang et al.[134] fabricated a similar sandwich-structured film using a relatively low pressure (3.3 kPa) (Figure 3c3). Their film preserved 45% of its d_{33} after a 24 h period at 90 °C. This suggests that the thermal stability of open-pore PTFE ferroelectrets surpass that of PP ferroelectret films. Wang et al.[64] prepared FEP–ePTFE–FEP films through hot pressing at 285 °C (Figure 3c4). The average pore size of ePTFE was 1 μm (Figure 3c5) and the thickness of FEP 12.5 μm. Their ferroelectret films still performed excellently nine months after charging, as listed in Table 1. Researchers have applied ePTFE with different porosities to fabricate sandwich-structured films with open pores.[132,135,136] The impact of porosity and layer thickness on charging voltage and piezoelectric performance of ferroelectret films will be discussed in Section 4. Shi et al.[137,138] made ferroelectrets with a rapid, low-cost method. They interlayered different polymer foams or conventional textiles with distinct Young's moduli with two FEP films, to achieve a d_{33} of 1000 pC N^{-1} and an output power of up to 62.4 μW cm^{-3}. The porosity of open-cavity structures is often higher than that of closed-cavity structures. This results in a lower Young's modulus, and makes them more suitable for detecting tiny forces.

A relatively novel method called freeze casting was also developed to get open pores. Zhang et al.[139] took up this technique to produce porous PVDF films, by dissolving PVDF powder in dimethyl sulfoxide (DMSO). The solution was unidirectionally frozen using liquid N$_2$, and the DMSO was then removed with water. Finally, the material was cut parallel to the freezing direction, resulting in long-range aligned pore channels with a pore size of 10 μm. The porous PVDF films attained after polarization a d_{33} coefficient of 264 pC N^{-1}.

3.3. Regular Cavity Structures

The control of the shape and size of the cavities created in polymeric films by the conventional methods discussed above is difficult, posing challenges to the optimization of the electromechanical properties of their ferroelectrets and their integration into microsystems.[140] Studies on charging and the resultant piezoelectricity highlight that quantitative control of the cavity structures through proper processing is crucial for maximizing the piezoelectric performance of ferroelectret films. Notably, polymers like COC, renowned for its ability to store positive charges faces difficulties in forming optimal cellular structures,[141,142] resulting in poor ferroelectret piezoelectric performance.[59] In recent years, in addition to open porous structures, regular

artificially engineered cavity structures have gained popularity for creating high-temperature-resistant ferroelectrets. This can be accomplished by mechanical processing, laser processing, 3D printing, etc. Particularly, 3D printing technology provides promising avenues for advancing ferroelectret research.
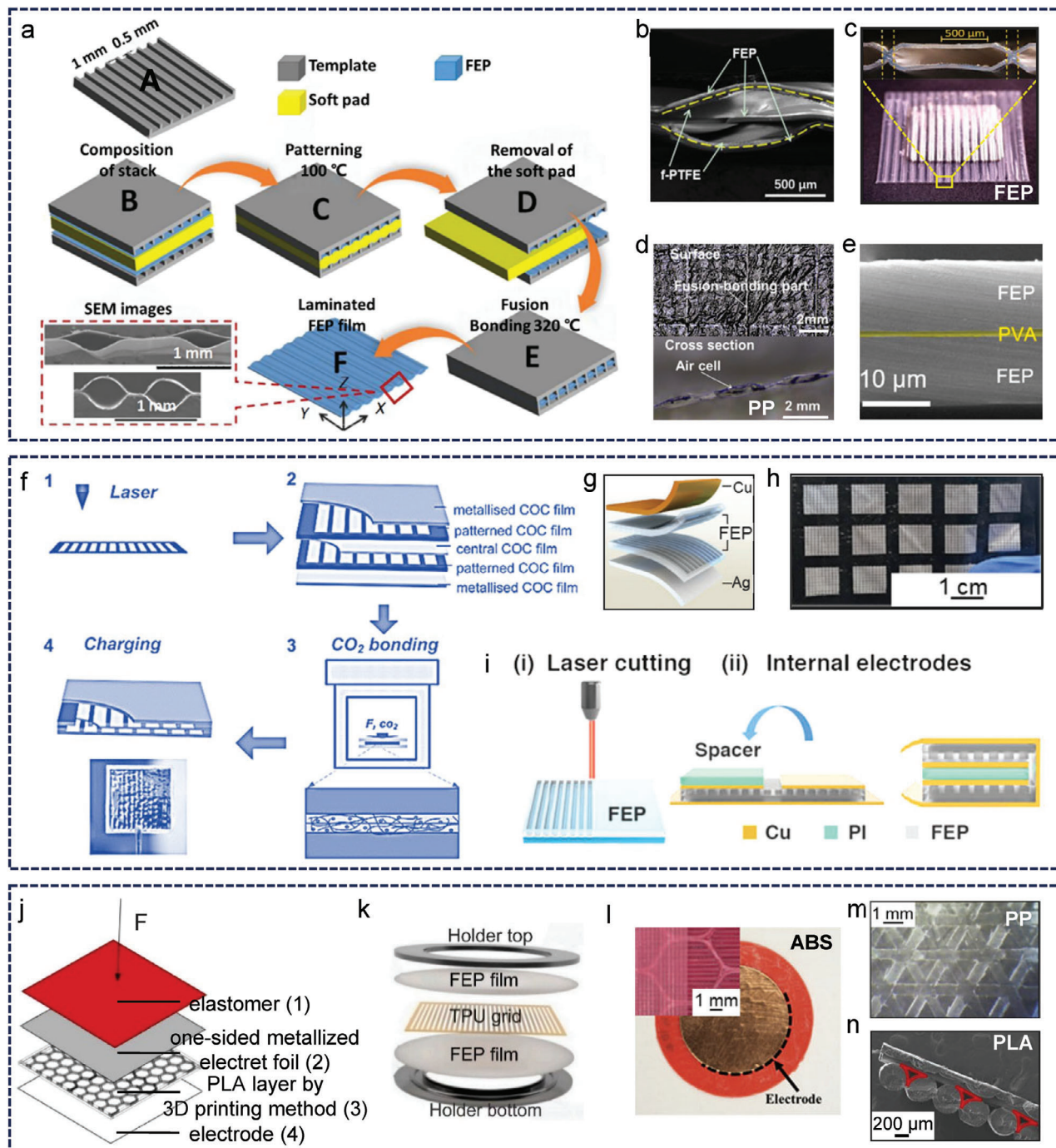
3.3.1. Mechanical Processing

Mechanical processing involves vacuum treatment,[143] hot pressing,[95,144] and needle perforation to form regularly distributed cavities in polymer films.[145] Altafim et al.[143] employed a vacuum-assisted thermal process to generate bubbles with a diameter of 1 mm between FEP films. They achieved a d_{33} of 500 pC N^{-1} after charging. Zhang et al.[103] combined mechanical molding with thermal bonding to build fluorinated-polymer ferroelectrets with regular cavities. By placing FEP film between a mold with regular grooves and a soft pad, as shown in **Figure 4a**, it is transformed into a wavy shape at 100 °C. Next, an array of tubular cavities is formed by hot-pressing at 320 °C. The resulting porous film has advantages of small footprints and high flexibility and is easy to produce. After charging, the tubular-arrayed film displayed an output energy of up to 109 μW, along with a low-frequency transverse piezoelectric coefficient g_{31} of no less than 3 Vm N^{-1}. Adopting a similar approach, Ma et al.[56,146,147] prepared a tube-like porous film based on FEP, to obtain acquired a quasi-static d_{33} as high as 4700 pC N^{-1}, which was maintained at 75% of its initial value after 14 days. The film responded within 80 ms as a sensor under a low pressure of 10 Pa. Wang et al.[136] thermally pressed a porous film composed of FEP with an f-PTFE interlayer (Figure 4b), to achieve an impressive d_{33} of up to 7380 pC N^{-1} after charging, by virtue of the excellent charge storage of f-PTFE. The manufacturing process and piezoelectric performance of the typical ferroelectrets mentioned in Section 3.3 are summarized in **Table 2**.

To create tubular cavities, several FEP tubes can be welded together in a mold at 270 °C. Zhukov et al.[148] made in this way an arrayed tubular-cavity FEP film with a wall thickness of 50 μm (Figure 4c) and got a piezoelectric d_{33} coefficient of 600 pC N^{-1}, comparable to that of PZT. Although the manufacturing process is simpler, the films produced have thicker cavity walls, which make their ferroelectrets inferior to those from other approaches. Ruan et al.[48] produced a highly transparent, ultrathin, skin-textured cavity-containing PP film stack (Figure 4d) with a quasi-static d_{33} exceeding 3000 pC N^{-1} by combining vacuum-assisted thermal processing with hot pressing.

Xu et al.[149] proposed electrostatic bonding as an alternative to hot pressing, where FEP layers, charged with opposite voltages, are separated with a patterned polyvinyl alcohol (PVA) layer in between to form a film stack with an open-cavity structure (Figure 4e). Wan et al.[145] employed a similar approach, putting an artificially perforated polyvinyl butyral (PVB) film in the middle. All these ferroelectret films perform well with also excellent biocompatibility. Lately, heterogeneous films prepared through mechanical machining have appeared.[150,151] This straightforward approach also resulted in highly flexible and piezoelectrically sensitive ferroelectret films.[152]

Mechanical processing often yields larger pores, resulting in lower elastic modulus of the film, which makes it more

Figure 4. Manufacturing of porous films with a regular, artificial cavity structure. a) Flowchart of mechanical processing. Reproduced with permission.[103] Copyright 2018, Elsevier Ltd. b) A five-layer porous film based on f-PTFE and FEP produced by hot pressing. Reproduced with permission.[136] Copyright 2016, Elsevier Ltd. c) FEP-based porous film with tubular cavities. Reproduced with permission.[148] Copyright 2018, Springer Nature. d) Optical images of the surface and cross-section of a skin-textured PP porous film. Reproduced with permission.[48] Copyright 2023, AIP Publishing. e) Cross-sectional SEM image of a sandwich-structured film with PVA as the dielectric layer. Reproduced with permission.[149] Copyright 2021, Elsevier Ltd. f) Flowchart of laser processing. Reproduced with permission.[154] Copyright 2013, Wiley-VCH GmbH & Co. KGaA. g) Hierarchical structure of FEP-based piezoelectret sensor, and h) optical image of laser-processed flexible porous films for mass production. Reproduced with permission.[155] Copyright 2022, Wiley-VCH GmbH. i) Diagram of laser processing of FEP-based porous film. Reproduced with permission.[157] Copyright 2023, Wiley-VCH GmbH. j) Exploded view of a ferroelectret nanogenerator fabricated by 3D printing. Reproduced with permission.[161] Copyright 2022, IEEE. k) Sandwich structure consisting of a 3D-printed TPU grid and FEP layers. Reproduced with permission.[163] Copyright 2021, MDPI. l) Optical image of 3D-printed ABS porous film with electrodes, with an inset illustrating its cavity structure. Reproduced with permission.[160] Copyright 2019, Elsevier B.V. m) Cavity structure of a 3D-printed PP porous film with triangular patterns. Reproduced with permission.[164] Copyright 2020, IEEE. n) Optical microscopy image of a 3D-printed PLA porous film. Reproduced with permission.[165] Copyright 2023, Elsevier B.V.

Table 2. Summary of various ferroelectret films with a regular cavity structure.

	Author	Polymer	Manufacture methods	d_{33} [pC N⁻¹]	Output power	Highlights
Mechanical processing	Altafim et al. (2006)[143]	FEP	A vacuum-assisted thermal process	500	–	Air cavities were created through vacuuming and heating assisted with a metal grid.
	Altafim et al. (2009)[144]	FEP	Hot pressing with PTFE template	160	–	Template-based tubular porous FEP film was proposed for easy producing and adjusting pore size.
	Zhang et al. (2018)[103]	FEP	Formed at 100 °C, then fusion bonding at 320 °C.	1300	109 μW	Wide frequency response from 10 to 35 Hz
	Ma et al. (2022)[56,146,147]	FEP	Fusion bonding at 320 °C after hot pressing	4700	–	Sensor exhibits rapid response time (80 ms) and low-pressure detection limit (10 Pa).
	Wang et al. (2017)[136]	FEP/f-PTFE	Formed at 100 °C, then fusion bonding at 280 °C.	7380	52 μW cm⁻²	Used mechanical processing to obtain a sandwich structure.
	Zhukov et al. (2018)[148]	FEP	Bonding FEP tubes together with a wall thickness of 50 μm.	600	–	The impact of tubular structures was studied.
	Ruan et al. (2023)[48]	PP	Bonding with an electric soldering iron after hot pressing with a PET mesh.	3000–6000	–	Simple manufacturing process, with a transparency of 80% and lightweight
	Xu et al. (2021)[149]	FEP–PVA–FEP	United by electrostatic force	930	–	Straightforward fabrication method
	Wan et al. (2022)[145]	FEP–PVB–FEP	Perforation by a tubular perforator and joined by electrostatic force.	4680	154.6 μW cm⁻²	High compatibility with biological tissues and a stable high output power
Laser processing	Basso et al.[153] (2007)	FEP–PTFE–FEP	Hot pressing at 3 10 °C after laser perforation	10	–	New approach for fabricating sandwich-structured porous films.
	Yan et al. (2013)[154]	COC	Assembled five layers COC by a CO_2 bonding (120 °C, 10 MPa) after laser machining.	1000	–	After heating at 110 °C for 200 h, the d_{33} maintains 70% of its initial value.
	Han et al. (2022)[155]	FEP	Hot pressing after laser engraving the patterns	5400	–	Used finite element simulation optimized the pattern and achieved better piezoelectric performance.
	Wang et al. (2012)[140]	PDMS	Stacking after the photoresist mold	300	–	Low elastic modulus of ≈500 kPa resulted in a high d_{33} of 300 pC N⁻¹.
	Wang et al. (2013)[156]	PDMS	Cellular structure was duplicated by a mold fabricated by a photoresist layer.	1000	–	Added an AF thin layer on the inner side of the cavities.
	Han et al, (2023)[157]	FEP–PI–FEP	Folded after laser cutting	591 pC kPa⁻¹	–	Employed a thicker folded bilayer structure to extend the high-sensitivity working range up to 8 kPa.
3D printing	Mirkowska et al. (2022)[161]	PP–PLA	Fused deposition modeling (FDM)	300	–	Used biodegradable PLA as intermediate layer.

(Continued)

**ADVANCED
SCIENCE NEWS**

www.advancedsciencenews.com

**ADVANCED
MATERIALS**

www.advmat.de

Table 2. (Continued)

Author	Polymer	Manufacture methods	d_{33} [pC N^{-1}]	Output power	Highlights
von Seggern et al. (2021)[163]	FEP–TPU–FEP	FDM	22 000	–	Ultrasoft TPU was applied as spacer and a high piezoelectric sensitivity was obtained.
Kierzewski et al. (2020)[160]	ABS	FDM	87	–	Sandwich structure with a porous layer of ≈200 µm thick
Assagra et al. (2021)[164]	PP	FDM	200	–	Integrated molding, yielding a d_{33} comparable to traditional ferroelectret foams.
Saini et al. (2023)[165]	PLA	FDM	350	–	Porous PLA film was fabricated by one-step molding.
Kumar et al. (2022)[167]	P(VDF-TrFE)	FDM	1200	440 µW cm^{-2}	Reduced cavity size to ≈170 µm and turned the ferroelectric polymer (PVDF) into a voided ferroelectret.

suitable for scenarios with lower applied forces compared to foaming methods. Although mechanical processing is costly for large-scale production in particularly when the pore structures are intricate, it does facilitate the fabrication of ferroelectret films with simple pore structures in high melting point polymers that are hard to foam.

3.3.2. Laser Processing

Laser processing involves the use of laser engraving to create specific arrayed geometric patterns on films, which are then stacked to a film arrangement with regular cavities. The shape of the pores can be precisely controlled through laser ablation. As listed in Table 2, Basso et al.[153] practiced laser technology to generate regularly patterned cavities on PTFE, which, acting as an intermediate layer, was thermally fused at 310 °C with two layers of FEP films to form a sandwiched cavity structure. The d_{33} was found to be only 10 pC N^{-1}, but it proved the feasibility of laser processing for creating cavity structure ferroelectret films.

Yan et al.[154] created long rectangle patterns on COC films by laser cutting. These films were then interleaved with pristine COC layers and bonded together in a CO_2 environment at 120 °C and 10 MPa (Figure 4f). Their porous film reached a d_{33} of up to 1000 pC N^{-1} which remained stable at 120 °C. This method presents advantages for mass production of ferroelectret films across a broad range of elastic moduli, structures, and temperatures. Similarly, Han et al.[155] created rectangular grooves on FEP films with laser engraving. They then interleaved and hot pressed two of these FEP films together to form ordered cavities (Figure 4g). Their ferroelectret films showed a remarkable d_{33} of 5400 pC N^{-1}, showcasing its substantial potential for mass production (Figure 4h).

Molds processed by lasers can be employed for the mass production of custom-made porous films with tailored piezoelectric properties. Wang et al.[140] created an array of cylindrical pores on a silicon wafer with photolithography. This served as a template for producing polydimethylsiloxane (PDMS) films with regular patterns. Next, two layers of the films were hot pressed together with a smooth PDMS layer. In this way, an array of cavities was formed. The charged porous PDMS film had a d_{33} of 300 pC N^{-1}. By incorporating a Teflon AF layer inside the cavities and leveraging its outstanding charge storage, the d_{33} was raised to 1000 pC N^{-1}.[156] Han et al.[157] created grooves on FEP by laser cutting, conjoined it with a polyimide (PI) film for folding into a porous sandwich (Figure 4i). Their ferroelectret showed a high sensitivity up to 8 kPa. This method is favored for its rapidity and simplicity, making it conducive to mass production. Despite its higher costs and the risk of material damage during laser ablation, laser processing offers superior capabilities for fabricating ferroelectret films with customized cavity structures, particularly for high-temperature-resistant polymers characterized by high elastic modulus.

3.3.3. 3D Printing

In recent years, 3D printing has emerged as prominent additive manufacturing technology, offering controllable complex

**ADVANCED
SCIENCE NEWS**

www.advancedsciencenews.com

**ADVANCED
MATERIALS**

www.advmat.de

shapes, high precision and low costs. 3D printing techniques such as fused deposition modeling (FDM/FFF), stereolithography (SLA), and digital light processing (DLP) are used for polymer molding;[108] however, SLA and DLP are less attractive for making porous films, because they require suitable photosensitive resins.[158] Early studies by Sborikas et al.[159] used screen printing to prepare polycarbonate (PC)-based cellular films with patterned photocurable ink as the middle layer. The d_{33} of their ferroelectret film amounted to a mere 28 pC N^{-1}, which remained stable up to 100 °C. It marked the first demonstration of the feasibility of additive manufacturing for the fabrication of sandwich-structured ferroelectret films. The designability and controllability of cavity profiles in 3D printing enable the fabrication of films with more intricate geometric shapes. This facilitates investigations into the influence of cavity patterns on the piezoelectricity of ferroelectrets.[105,160]

Mirkowska et al.[161] proposed a straightforward stacking for making chargeable porous structures. The layers, arranged in sequence, include an elastomer layer, one-sided metalized electret film, a 3D-printed lattice PLA layer and electrodes (Figure 4j). Their porous film exhibited a d_{33} of 300 pC N^{-1}, comparable to that of traditional ferroelectret films, as listed in Table 2. Clearly, the charge storage is determined predominantly by the electret film, while the mechanical properties depend mainly on the elastomer layer. The charge stability of porous PLA films with a layered structure has also been explored by others.[162] Von Seggern et al.[163] took a 3D-printed lattice made of ultrasoft thermoplastic polyurethane (TPU) as an intermediate layer (Figure 4k). Their charged ferroelectret film showed a remarkable d_{33} of 22 000 pC N^{-1}. This value largely derives from the extremely low Young's modulus of TPU. The reason for its impact on the electromechanical behavior of the ferroelectret film will be addressed by charge-spring model in Section 4.1.3.

In addition, integrated printing of porous films was shown possible. Kierzewski et al.[160] used acrylonitrile butadiene styrene (ABS) as a substrate and chose a hexagonal infill pattern to create ABS porous films with accessible pores (Figure 4l). The piezoelectric action of three different filling ratios was studied. This showed that lower filling ratios lead to better piezoelectric performance. A ferroelectret film with a filling ratio of 2.5% demonstrated a d_{33} of 262 pC N^{-1}. Assagra et al.[164] employed a triangular infill pattern for PP films and obtained designed porous PP films (Figure 4m). The d_{33} reached 200 pC N^{-1} after charging, higher than that of PP ferroelectrets prepared by conventional foaming.

Saini et al.[165] produced films with smaller-sized cavities by taking biodegradable PLA as the substrate. They employed a layer-by-layer printing with rod-like shapes, leading to semicrystalline PLA films with a regular porosity (Figure 4n). These films attained a piezoelectric d_{33} coefficient of 350 pC N^{-1} after polarization. Perna et al.[166] adopted a similar approach to print porous films with a porosity of 77% using 3D-printable commercial PLA. They obtained a piezoelectric coefficient of 212 pC N^{-1} after polarization. The method can also be applied for making porous P(VDF-TrFE) films, a piezoelectric d_{33} coefficient as high as 1200 pC N^{-1} was obtained due to the softer porous structure combined with the molecular dipoles.[167] Other researchers have invoked 3D printing to obtain porous structures from polymers such as COC.[60]

While 3D printed ferroelectrets have achieved favorable piezoelectric properties, the overall performance remains inferior to that of samples made by the methods reviewed earlier. Hence there is still room for improvement in manufacturing ferroelectrets with regular cavities by 3D printing. This can be achieved with a higher printing accuracy and use of advanced methods like DLP and SLA.

Recently, origami folded structures have been investigated for the fabrication of triboelectric nanogenerators.[168,169] Such special compact folded structures allow multiple dielectric layers to move a large distance when subjected to a small force. This generates an electric current, because the charge induced on the electrodes changes upon contact and separation of the electret layers. When cavities are incorporated inside the origami-inspired electrets, the macroscopic dipole moment will change even more upon compression. Artistically folded ferroelectrets may therefore have great potential for highly sensitive sensors.

Recapitulating, regular cavities offer opportunities for enhancing the ferroelectret properties by tailoring them to specific tasks.

4. Piezoelectric Enhancements of Ferroelectrets

4.1. Theoretical Models of Piezoelectric Coefficients

4.1.1. Closed-Cavity Structure

In 1999, Sessler and Hillenbrand[170,171] developed a model for analyzing the piezoelectric coefficients of charged cellular films. When a stress is applied, the lateral deformation of cavities is significantly less than the longitudinal deformation because of the highly anisotropic mechanical properties of ferroelectret films. Therefore, the closed-cavity structure was simplified to a multilayered system, composed of alternate solid and air layers with thicknesses d_{1i} and d_{2j}, respectively, where $i = 1, 2, \cdots, n$ and $j = 1, 2, \cdots, n-1$, and n is the total number of solid layers (**Figure 5a**).

The relation between interlayer charge density σ_j and the different layer thicknesses can be established using Gauss' law and Kirchhoff's second law

$$E_1 = E_{11} = E_{12} = \cdots = E_{1k} = \frac{\sum_j d_{2j}\sigma_j}{\epsilon_0\left(d_1 + \epsilon_s d_2\right)} \tag{2}$$

$$E_{2i} = \frac{\sigma_i}{\epsilon_0} - \frac{\epsilon_s \sum_j d_{2j}\sigma_j}{\epsilon_0\left(d_1 + \epsilon_s d_2\right)} \tag{3}$$

where $d_1 = \sum_i d_{1i}$ and $d_2 = \sum_j d_{2j}$ represent the total thicknesses of the walls and air layers of the cavities, respectively. Note ϵ_0 is the permittivity of vacuum, while the dielectric constant of the air is 1 and that of the solid polymer part is ϵ_s.

The induced charges on the top and bottom electrodes can be expressed as

$$\sigma_0 = \epsilon_0 \epsilon_s E_1 \tag{4}$$

Clearly, E_1 will change upon deformation of the porous film. Part of this change will be brought about by the change in thickness of the air layers d_{2j}. It can be expected that

$$\frac{\partial d_{2j}}{\partial d_2} = \frac{d_{2j}}{d_2} \tag{5}$$
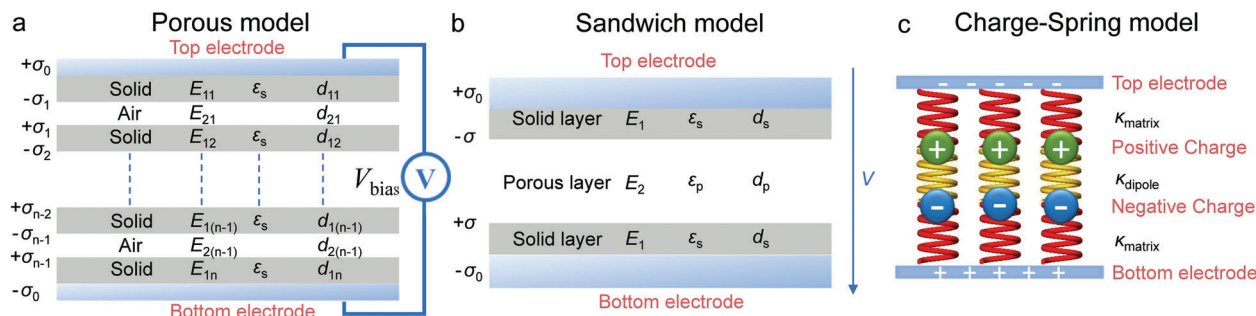
Figure 5. Simplified models for ferroelectrets. a) Model of porous ferroelectret films with alternate polymer and air layers. Reproduced with permission.[170] Copyright 1999, IEEE. b) Model of open cavity ferroelectret films with two dielectric outer layers and a highly elastic layer in the middle. Reproduced with permission.[104] Copyright 2011, IEEE. c) Charge-spring model with matrix phase, dipole phase, and interfacial charges. Adapted with permission.[174] Copyright 2014, IEEE.

Substituting Equation (2) into Equation (4) will then yield, when the cavities undergo a longitudinal deformation due to external forces, for variation in the induced charges on the upper and lower electrodes

$$\frac{\partial \sigma_0}{\partial d_2} = \frac{\varepsilon_s d_1 \sum_j d_{2j} \sigma_j}{d_2 \left(d_1 + \varepsilon_s d_2\right)^2} \tag{6}$$

Hooke's law gives Young's modulus Y of the film

$$\frac{\Delta d_2}{d} = \frac{p}{Y} \tag{7}$$

where p is the stress applied to the film and $d = d_1 + d_2$ is the overall thickness of the film.

The piezoelectric d_{33} coefficient of the cellular ferroelectret film can be found from

$$d_{33} = \left(\frac{\partial D_3}{\partial T_3}\right)_E = \frac{\Delta \sigma_0}{p} = \frac{\varepsilon_s d}{Y} \frac{d_1 \sigma_{eff}}{\left(d_1 + \varepsilon_s d_2\right)^2} \tag{8}$$

where $\sigma_{eff} = \frac{\sum_j d_{2j} \sigma_j}{d_2}$ is the effective polarization of the ferroelectret film.

In the meantime, Paajanen et al.[172,173] also proposed a model that incorporated the effect of a bias voltage (V_{bias}) on the piezoelectric coefficient (Figure 5a). It results in a d_{33} given by

$$d_{33} = \frac{\Delta \sigma_0}{p} = \frac{\varepsilon_s d}{Y} \frac{d_1 \sigma_{eff} - \varepsilon_0 \varepsilon_s V_{bias}}{\left(d_1 + \varepsilon_s d_2\right)^2} \tag{9}$$

d_{33} will thus increase, if the polarity of V_{bias} and σ_{eff} differ.

Equations (8) and (9) indicate that the piezoelectric sensitivity of ferroelectrets is primarily governed by the Young's modulus of the foam, the respective permittivity and thickness of the polymer layers and air layers, and the effective polarization. It is worth noticing that the model does not show how the varying charge capture capabilities of materials affect the charge density. This requires further investigation.

4.1.2. Sandwich Structure with Open Cavities

Kacprzyk et al.[62] proposed a simple model of a double-layer dielectric to estimate its d_{33} coefficient and achieved a satisfactory prediction. With the advancement of flexible ferroelectret films, there came the sandwich structures with open cavities such as FEP–ePTFE–FEP, which showed an exceptional piezoelectric performance. Zhukov et al.[80] developed a charging model for this three-layered sandwich structure (Figure 5b).

Gauss' law can be expressed as follows at the upper and lower electrodes by

$$\varepsilon_0 \varepsilon_s E_1 = \sigma_0 \tag{10}$$

while at the upper and lower boundaries of the ePTFE-part in the ferroelectret we have

$$\varepsilon_0 \varepsilon_s E_1 - \varepsilon_0 \varepsilon_p E_2 = -\sigma \tag{11}$$

Note ϵ_p being the relative permittivity of the porous part and ϵ_s that of the solid polymer part.

In the context of a short-circuit scenario with $V = 0$, Kirchhoff's second law can be expressed as

$$2E_1 d_s + E_2 d_p = 0 \tag{12}$$

By substituting Equations (10) and (12) into Equation (11), one gets

$$E_1 = -\frac{\sigma d_p}{\varepsilon_0 \left(d_p \varepsilon_s + 2 d_s \varepsilon_p\right)} \tag{13}$$

In accordance with the stress–strain relation from Equation (7), the piezoelectric d_{33} coefficient can be calculated through combining Equations (10) and (13)

$$d_{33} = \frac{2 d d_s \varepsilon_s \varepsilon_p \sigma}{Y \left(d_p \varepsilon_s + 2 d_s \varepsilon_p\right)^2} \tag{14}$$

where $d = 2 d_s + d_p$. The d_{33} obtained clearly is proportional to the residual charge σ within the solid layer, and hence is closely related to the charging process. Zhukov and von Seggern investigated the impact on the piezoelectric effect of porosity and geometric shapes of the intermediate porous layer. They established the following relation between the maximum residual charge and the breakdown voltage (V_B) in the intermediate layer[90]

$$\sigma_{max} = \left(\varepsilon_p \varepsilon_0 + \varepsilon_s \varepsilon_0 \frac{d_p}{2 d_s}\right) E_B \text{ for } V \geq 2 V_B \tag{15}$$

**ADVANCED
SCIENCE NEWS**

www.advancedsciencenews.com

**ADVANCED
MATERIALS**

www.advmat.de

where $E_B = V_B/(d_p + \frac{2\varepsilon_p d_s}{\varepsilon_s})$ represents the electric field within the intermediate layer as soon as the charging voltage exceeds the breakdown voltage. The breakdown field depends on the cavity size, the thicknesses and dielectric constants of the porous and solid layer. When the polarization voltage is less than twice the breakdown voltage, cf., Figure 2d, the residual interface polarization charge cannot reach its maximum value.[80]

By substituting Equation (15) into Equation (14), it can be deduced that the maximum d_{33} is reached when the charging voltage exceeds twice the breakdown voltage

$$d_{33}^{max} = \frac{\varepsilon_0 \varepsilon_s \varepsilon_p (2d_s + d_p)}{Y(d_p \varepsilon_s + 2d_s \varepsilon_p)} E_B \tag{16}$$

Zhukov et al.[80] further confirmed that reducing the porosity of the intermediate layer will enhance E_B. It also implies a higher elastic modulus and requires a higher voltage for charging. Making use of the fact that the deformation of the intermediate layer is substantially larger than that of the solid layers when the film is under compression. Von Seggern et al.[86] derived a relation between the Young's moduli of the film (Y) and the intermediate layer (Y_p), along the thickness direction. This ultimately leads to a simple expression for d_{33}^{max}

$$d_{33}^{max} = \frac{\varepsilon_0 \varepsilon_s \varepsilon_p}{Y_p \left(\varepsilon_s + \frac{2d_s}{d_p} \varepsilon_p\right)} E_B \tag{17}$$

It shows that reducing the thickness ratio between the solid layer and the porous intermediate layer will strengthen the piezoelectric performance. In short, this model relates the mechanical properties, charging conditions, and piezoelectric performance of sandwich-structured ferroelectret films. Zhukov et al.[80] observed that the breakdown field, the primary factor determining the piezoelectric coefficient of sandwich films, rises as the porosity and thickness of the porous layer decrease. They further validated the model experimentally using sandwich-structured specimens of different solid layer thicknesses and different permittivities.

4.1.3. Charge-Spring Model for Ferroelectrets

The two models discussed above focus primarily on the charges induced on the electrodes by changes in dipole moment. The piezoelectric effect generated can be attributed to two mechanisms: one involves the linear variation of the dipole moments caused by an applied stress ("primary piezoelectricity"), while the other involves the linear variation in the density of dipoles by the applied stress ("secondary piezoelectricity").[174] To further investigate the piezoelectric behavior of space charge and dipolar polarization, Gerhard introduced a charge-spring model for heterogeneous medium with embedded charges. This model encompasses two phases, the matrix and dipole phase, as depicted in Figure 5c, in which they are represented by different springs. The microscopic charges and springs can be lumped together into macroscopic charge layers or polarizations and macroscopic elastic moduli or compliances.[174]

If we consider the specific case where a ferroelectret film experiences compression only in the thickness direction, a series of derivations lead to following expression for the d_{33} coefficient

$$d_{33} \approx -\frac{P_3}{Y_m} + \frac{P_3}{Y_d} \tag{18}$$

where P_3 is the component of the polarization vector in the thickness direction, Y_m and Y_d are the elastic moduli of the matrix and dipole phase, respectively.

The expression for d_{33} obtained from the charge-spring model thus incorporates the elastic moduli of the matrix phase and dipole phase of ferroelectrets. The dielectric constant of the materials and pore size are not explicitly included. However, their influence on d_{33} is accounted for by the polarization vector and the Young's moduli. It thereby offers a new approach to enhance the piezoelectric performance of ferroelectrets, namely, increase the disparity between the elastic moduli of the two phases. This can be achieved by adjusting the processing parameters to regulate pore shape and size, by controlling the stretching force, gas expansion pressure, and heat treatment temperature in biaxial stretching, using softer or harder intermediate layers in sandwich structures and changing the design parameters for regular cavities. Furthermore, Wang et al.[175] calculated the elastic modulus of ePTFE dipole phases using Equation (18) after measuring the piezoelectric d_{33} coefficients and the remnant polarizations. Due to the large reduction in the porosity of ePTFE by the hot-pressing process, the modulus obtained, was slightly higher than reported in the literature, but within the same order of magnitude. The validity of the model was thus verified.

The charge-spring model presents a much more general approach that can be applied to all piezoelectric materials and that might be extended to pyroelectricity.[176,177] It is furthermore helpful for teaching purposes, as the concept of charges and springs can be understood and visualized easily.

4.2. Mechanisms and Methods for Improving Piezoelectric Performance of Ferroelectrets

4.2.1. Optimal Design of Foam Structure

The impact of cavity geometry and film porosity on the piezoelectric performance of ferroelectrets is vast. Several studies were therefore aimed on optimizing the cavity structure for elevating the piezoelectric properties.[139,178] It has been shown that variations in cavity geometries and porosities result in a change in piezoelectric response for closed-cavity structured ferroelectret films.[69,81,117,121] Harris and Mellinger[179] investigated the charging of cellular PP films with different cavity sizes, noting that the light emissions were emanated homogeneously for cavity heights ranging from 8 to 25 μm. Wegener et al.[81,180] conducted a series of experiments and prepared PP films with different cavity geometries by controlling the gas expansion pressure and heat treatment temperature during the inflation process. They found that as the film density changes, the piezoelectric d_{33} coefficient reaches its maximum when the elastic modulus is at its minimum. This occurs at a film density of 0.41 g cm^{-3} and an elastic modulus of 1.3 MPa for cellular PP with lens-shaped cavities

**ADVANCED
SCIENCE NEWS**

www.advancedsciencenews.com

**ADVANCED
MATERIALS**

www.advmat.de
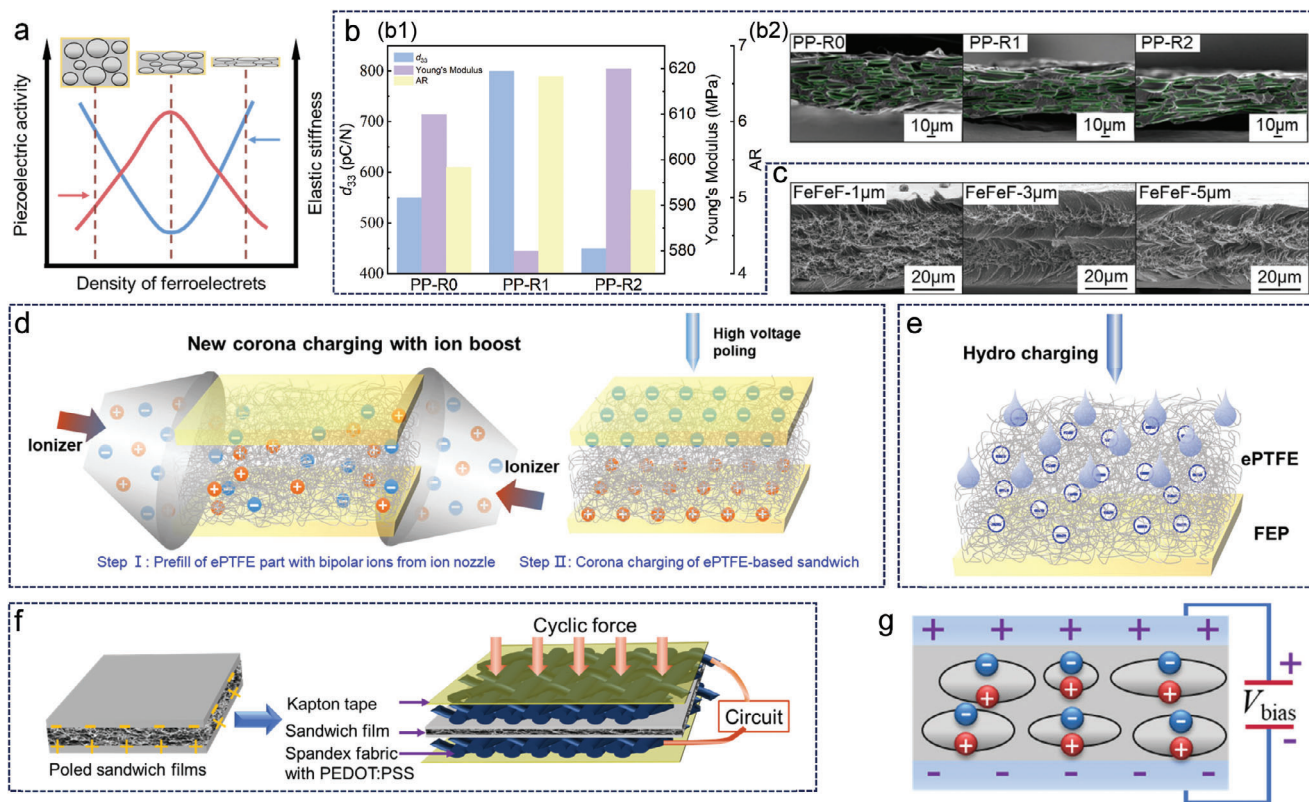
Figure 6. Mechanisms and methods for improving piezoelectric performance of ferroelectrets. a) Relation between piezoelectric activity, elastic stiffness, and cross-sectional cellular structure of typical closed-cavity ferroelectrets. Reproduced with permission.[81] Copyright 2005, Wiley-VCH GmbH & Co. KGaA. b) Influence of the cavity structure in PP ferroelectrets on the piezoelectric performance for three cavity sizes. b1) The corresponding d_{33}, Young's moduli and aspect ratio (AR), along with b2) cross-sectional SEM images of the three PP ferroelectrets. Reproduced with permission.[110] Copyright 2016, Wiley Periodicals. c) Cross-sectional SEM images of five-layer ferroelectret films with average pore sizes of 1, 3, and 5 μm in ePTFE. Reproduced with permission.[64] Copyright 2021, Wiley-VCH GmbH. d) Schematic of ion-prefilling for boosting the polarization of ePTFE-based sandwiches. Reproduced with permission.[91] Copyright 2022, American Chemical Society. e) Illustration of hydrocharging for sandwich-structured porous films. f) Diagram of charged ePTFE-based sandwich structure with fabric electrodes. Reproduced with permission.[64] Copyright 2021, Wiley-VCH GmbH. g) Illustration of application of DC bias voltage for porous films.

(**Figure 6**a). Mohebbi et al.[110] obtained porous PP films with a normal cavity structure through uniaxially stretching (designated as PP-R0), and two distinct cavity structures by hot-pressing treatments, labeled PP-R1 and PP-R2. The PP film, named PP-R1, was processed by gradually increasing the temperature to 105 °C in stages within 20 min while simultaneously increasing the pressure gradually to 5 MPa, followed by a 10 min hold period, and then cooled down. In contrast, the PP film, named PP-R2, was heated to 105 °C within 10 min while gradually increasing the pressure to 5 MPa. The longitudinal (L) and transverse (T) cross-sectional SEM images are depicted in (Figure 6b2). PP-R1 had the highest aspect ratio (AR), along with the lowest Young's modulus and highest d_{33} (Figure 6b1). The latter result is consistent with predictions of the spring-charge model from Gerhard.[174] This predicts higher piezoelectric coefficients if the Young's modulus of the compliant dipole phase decreases. Zhang et al.[103] fabricated an array of tubular cavities in FEP films using mechanical machining. This resulted in significantly higher d_{33} values of 1300 pC N^{-1}, compared to regular porous FEP ferroelectrets, as shown in **Table 3**. The large d_{33} arises from the smaller Young's modulus.

For FEP–ePTFE–FEP sandwich ferroelectrets, Wang et al.[64] studied the effect of pore size and film thickness of the ePTFE layer, as well as the number of macrodipoles in series (Figure 6c). They found that the piezoelectric performance increases with the thickness of the porous layer and concluded that the stacking sequence FEP–ePTFE–FEP–ePTFE–FEP with an ePTFE pore size of 3 μm displays the best piezoelectric performance, cf. Table 3. This is attributed to the optimal combination of number of macrodipoles and low overall Young's modulus.

4.2.2. Ion-Boosting Methods

According to the theoretical models of Section 4.1, the piezoelectric activity is proportional to the charge density on the internal surfaces of the cavities (effective polarization). The charging efficiency can be enhanced considerably by filling the cavities with extra ions during charging. This can be realized through photoionization of the air molecules inside the cavities with soft X-rays.[181,182] Furthermore, the application of a high-frequency AC voltage with an amplitude close to the breakdown threshold of

**ADVANCED
SCIENCE NEWS** _____
www.advancedsciencenews.com

**ADVANCED
MATERIALS**
www.advmat.de

Table 3. Summary of various effective polarization-enhancing methods for ferroelectrets.

	Author	Polymer	Manufacture methods	d_{33} [pC N^{-1}]	Output power	Highlights
Optimization of foam structure	Wegener et al. (2004)[117]	PP	A two-step inflation process (N$_2$ 5 MPa)	590	–	Controlled short heat treatment improves the piezoelectric properties.
	Zhang et al. (2018)[95]	FEP	Stacking and hot pressing after mold processing	1000	250 µW cm^{-2}	High output power, broad bandwidth, and excellent fatigue performance
	Zhang et al. (2018)[103]	FEP	Formed at 100 °C, then fusion bonding at 320 °C.	1300	109 µW	Wide frequency response (10–35 Hz)
	Wang et al. (2021)[64]	FEP–ePTFE–FEP–ePTFE–FEP	Hot pressing (285 °C, 5 kN, 1–2 h)	–	4.5 µW cm^{-2}	Compared piezoelectric performance of ferroelectrets for different pore sizes of ePTFE and stacking structures.
Ion-boosting methods	Wang et al. (2022)[91]	FEP–ePTFE–FEP–ePTFE–FEP	Hot pressing (285 °C, 5 kN, 0.5–1 h)	1600	4 µW cm^{-2}	Injecting extra ions generated by an in-line ionizer before the corona poling.
	Wang et al. (2022)[91]	FEP–ePTFE–FEP	Hot pressing (285 °C, 5 kN, 0.5–1 h)	240	–	Blowing in negative ions into the porous layer during polarization using a negative ion blower.
Porous fabric electrodes	Wang et al. (2021)[64]	FEP–ePTFE–FEP	Hot pressing (285 °C, 5 kN, 1–2 h)	–	1.5 µW cm^{-2}	PEDOT:PSS-coated spandex fabric was applied as electrodes.
Application of DC bias voltage	Hillenbrand and Sessler (2008)[189]	PP	A double-expansion process after biaxial stretching	1200	–	Significantly increased the d_{33} coefficient of PP ferroelectret films by DC bias of 1500 V.
Synergy effect	Ghosh et al. (2016)[195]	P(VDF-HFP)	Chemical foaming with Pt-NPs doping	836	0.53 µW cm^{-2}	Under pressure of a finger (1.1 MPa), a high open-circuit voltage (6 V) and short-circuit current can be obtained (6.4 µA).
	Xu et al. (2018)[196]	PVDF	Chemical foaming with doping with GQD as dopant	–	≈8.5 nW cm^{-2}	Simple fabrication, self-polarization, and high piezoelectric performance
	Zhang et al. (2019)[139]	PVDF	Freeze casting with liquid N$_2$	264	–	Pioneering work of PVDF ferroelectret with long-range alignment of pore channels

the gas in the cavities together with the DC poling voltage can effectively mitigate plasma degradation within the cavities.[183]

Wang et al.[91] found that the piezoelectric performance can also be boosted simply by injecting additional ions into the open-cavity structure of the intermediate layer of a sandwich-structured ferroelectret during the charging process (Figure 6d). Excessive ions were generated from clean air with an in-line ionizer, and injected laterally into the sandwich structure through the interconnected open pores of the ePTFE layer. Upon further separation of injected ions, the FEP–ePTFE–FEP–ePTFE–FEP film charged with additional ions raised d_{33} to a level as high as 1600 pC N^{-1}, four times higher than that of the same film poled with the normal corona charging, as listed in Table 3.

Wang et al.[91] injected furthermore negative ions into the open porous structure of an ePTFE layer in an ePTFE–FEP laminate using a negative ion blower during negative corona poling. Covering this bootstrapped charged bilayer with an unpoled solid layer of FEP, an FEP–ePTFE–FEP structure was obtained. They found that the piezoelectric coefficient of the prepared unipolar ferroelectret amounted to a d_{33} of 240 pC N^{-1}, three times higher than that of an FEP–ePTFE–FEP film charged using the standard negative corona charging.

Hydrocharging involves spraying water onto the surface of fabric fibers through very high-pressure water jetting (Figure 6e). This technique has recently been applied in the production of charged melt-blown fabrics and was proven to increase the filtration efficiency of melt-blown polypropylene microfiber filters by more than twice to that of filter webs charged by corona charging.[184,185] Therefore, hydrocharging may also have a potential as a new effective approach for the charging of ferroelectrets as well, particularly when the water is sprayed into the open cavities not as a powerful jet, but as an aerosol of charged microdroplets.[186]

4.2.3. Porous Fabric Electrodes

Generally, the electrodes used for ferroelectrets are metal-based. Wang et al.[64] reported a surprisingly high output power of an FEP-ePTFE-FEP nanogenerator with poly(3,4-ethylenedioxythiophene):poly(styrene sulfonate) (PEDOT:PSS)-coated spandex fabric electrodes, nearly three times higher than that of the same film with aluminum foil electrodes (Figure 6f), as listed in Table 3. Hence, the piezoelectric performance of a

ADVANCED
SCIENCE NEWS

www.advancedsciencenews.com

**ADVANCED
MATERIALS**

www.advmat.de

ferroelectret film can be improved by replacing the metal electrodes with a conductive fabric, which is also a kind of porous material. The fabric electrode itself forms an additional charge-spring dipole layer by the appearance of induced charges owing to its inherent porous structure. It acts as an additional piezoelectric-transducer element in view of the fact that the adjacent electret film carries a surface charge. It therefore lifts up the overall performance of the ferroelectret film by adding in series one additional charge-spring layer.

Vapor deposition was first employed by Zhang et al.[187] as coating technique for making fabric electrodes. Such electrodes possess intrinsic textile properties such as flexibility, wear resistance, breathability along with a tactile feel accepted by users. Furthermore, they exhibit a linear resistivity. The technique involves coating a conductive polymer PEDOT onto the fabric, followed by vapor-phase polymerization in a reactive vapor deposition chamber. After a series of cleaning and annealing steps, a final nonmetallic fabric electrode is obtained. Obviously, the human body-friendly fabric electrodes could improve the overall piezoelectric performance to propel the use of ferroelectret films in wearable devices.

4.2.4. Application of DC Bias Voltage

According to Equation (9), a bias voltage will contribute to the d_{33} coefficient. When V_{bias} is much smaller than the breakdown voltage of the gas within the cavities, σ_{eff} remains unchanged. In this case, d_{33} grows linearly with the bias voltage. Qiu et al.[83,188] studied by means of acoustical measurements the build-up of the effective polarization in ferroelectrets under bipolar voltage waveforms. This study proved that the acoustic signal emitted by ferroelectrets under an AC driving voltage can be improved markedly by superimposing it with a DC bias voltage (Figure 6g). As listed in Table 3, Hillenbrand and Sessler studied the d_{33} coefficient of piezoelectrets under DC bias voltages with an interferometer.[189] They obtained very high d_{33} coefficients of up to 1200 pC N^{-1} by applying a DC bias voltage of 1500 V, whereas without DC bias d_{33} was ≈500 pC N^{-1}. Döring et al.[190–192] investigated the ultrasonic transmission between two air-coupled PP piezoelectret transducers under high-voltage exciting pulses. Pulses of 3500 V led to large enhancements in the transducer constant (a factor of 3), the air-coupled ultrasonic transmission (12 dB), and the signal-to-noise ratio (32 dB). Gaal et al.[193] studied PP piezoelectret transducers under biasing conditions for nondestructive testing the internal structure of a rotor blade segment and glued-laminated timber. They achieved an increase in the signal-to-noise ratio of up to 15 ± 1 dB by applying a DC bias of 2 kV. These studies clearly demonstrate the enhancement in piezoelectric performance by invoking a DC bias.

4.2.5. Synergy of Foam Structure and Ferroelectric Effect

The striking piezoelectric performance of ferroelectret films derives from highly compressible, large macrodipoles formed in the porous structure by charging. This kind of porous structure can also be applied to strengthen the performance of a PVDF ferroelectric polymer.[194] Ghosh et al.[195] combined the ferroelectret characteristics of a voided structure with the genuine dipolar

ferroelectric phenomenon of PVDF films. They made a porous PVDF ferroelectric film through chemical foaming and incorporated platinum nanoparticles (Pt-NPs) to induce the generation of electrically active β-PVDF. Xu et al.[196,197] filled the cavities of porous PVDF with a solid perfluorosulfonate ionomer (Nafion). They doped porous PVDF with graphene quantum dots (GQDs) and investigated the role of doping concentration on the piezoelectric performance. These films exhibit not only a prominent piezoelectricity but also characteristics of ease of fabrication and self-polarization, cf. Table 3. Zhang et al.[139] prepared a special kind of porous PVDF by freeze casting, which displays a favorable d_{33} coefficient (264 pC N^{-1}) after charging. PVDF is a polar ferroelectric polymer with an inferior space-charge stability. Space charges in PVDF are short-lived, they can be estimated to last for roughly 1000 s.[198,199] Therefore, one can expect that a fair share of the macroscopic dipoles in porous PVDF will vanish after poling due to the decay of the space charges deposited on the inner surfaces of the cavities. The high d_{33} coefficient of cellular PVDF film may on that account be attributed to the joint integration of molecular dipoles and very soft porous structure.[174] From Equation (18), one gets $d_{33} = -P_3/Y_m$ by considering only the dipole-density effect. If one neglects the influence of the foaming process on the molecular dipoles and the crystallinity of PVDF films, one has $P_{3,porous} = (1-p)P_{3,solid}$, where $P_{3,porous}$ and $P_{3,solid}$ are the polarization of porous and solid PVDF films, respectively, and p is the porosity of the porous PVDF film. As a matter of fact, $P_{3,porous}$ is smaller, but still more or less of the same magnitude as $P_{3,solid}$. However, the Young's modulus of porous polymer films might be orders of magnitude lower than that of their solid counterparts. All in all, the moderately reduced polarization in combination with the hugely lowered Young's modulus might explain the high d_{33} of porous PVDF. But more solid data than currently available in the literature are needed to confirm this assumption. It should be pointed out that the origin of piezoelectricity is quite different for nonpolar ferroelectrets and polar ferroelectrics. In ferroelectrets with macroscopic dipoles (internally charged cavities), the dipole phase is much more compressible than the polymer matrix, and hence ferroelectrets exhibit a primary piezoelectric effect (dipole-moment piezoelectric effect). In ferroelectric polymers such as PVDF with microscopic dipoles (oriented molecular dipoles), the dipoles are stiff, while the amorphous matrix is much softer. PVDF shows secondary piezoelectricity (dipole-density piezoelectric effect). Consequently, ferroelectrets exhibit a positive d_{33} and negative d_{31} and d_{32}, while PVDF has a negative d_{33} and positive d_{31} and d_{32}. The piezoelectric coefficients in ferroelectrets are thus opposite to those of ferroelectric polymers. Therefore, we should realize that macroscopic dipoles and microscopic dipoles in porous ferroelectric polymers counteract each other's contribution to the piezoelectric effect, rather than reinforcing it. It should further not come as a surprise, when the sign of d_{33} would switch with time, because the two opposing contributions will for sure decay at a different rate. Polar polymers offer no advantage over nonpolar ones in this respect.

Despite the needs of additional mechanism study due to the complex interplay between interface charges and molecular dipoles in PVDF,[198,199] this synergy of foam structure and inherent ferroelectric effect of PVDF appears attractive in boosting the low piezoelectric performance in solid PVDF for a broader application.

**ADVANCED
SCIENCE NEWS**

www.advancedsciencenews.com

**ADVANCED
MATERIALS**

www.advmat.de
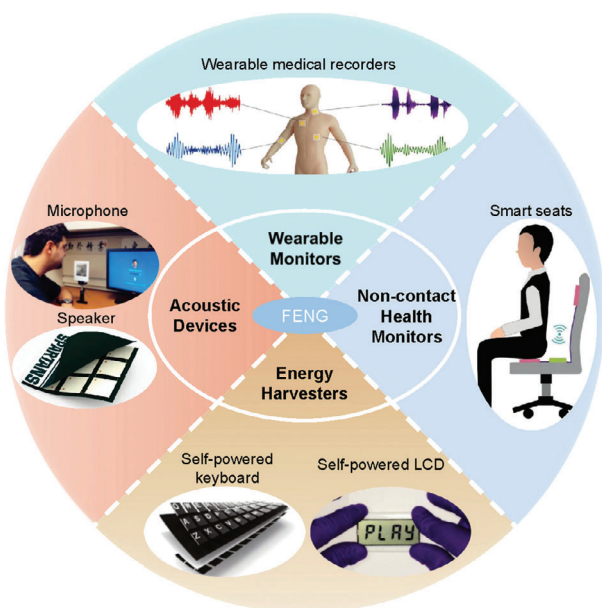
Figure 7. Recent applications of ferroelectret films in acoustic devices. Reproduced with permission.[202] Copyright 2016, Springer Nature. Wearable monitors. Reproduced with permission.[157] Copyright 2023, Wiley-VCH GmbH. Noncontact health monitors. Reproduced with permission.[206] Copyright 2022, Tsinghua University Press. Energy harvesters. Reproduced with permission.[100] Copyright 2016, Elsevier Ltd.

5. Applications of Ferroelectrets

The piezoelectric and mechanical performance of ferroelectret films depend strongly on their diverse structures. Variations in materials and cavity structures lead to significant disparities in ferroelectret performance. As a result, ferroelectret films with distinct characteristics are being applied in various fields, albeit primarily in acoustic devices,[200–202] wearable health and motion monitors,[157,203,204] noncontact health monitors,[205,206] and energy harvesters (**Figure 7**).[100,207,208]

5.1. Acoustic Devices

Acoustic devices represent a traditional application of piezoelectric materials. Hillenbrand and Sessler studied piezoelectret microphones made of gas expanded cellular PP films.[209,210] They found that single-film and five-stacked-film microphones have sensitivities of ≈2 and 10.5 mV Pa^{-1} at 1 kHz. The latter is comparable to that of electret condenser microphones. Ferroelectret microphones have many advantages such as simple design, low cost, light weight, and flexibility, making them suitable for a wide range of applications. Li et al.[202] fabricated dual-functional speakers and microphones using cellular PP ferroelectrets (**Figure 8a,b,c1**). Measurements on the directional sound pressure levels of various configurations confirmed that cellular PP ferroelectret speakers perform very much like traditional acoustic products (Figure 8c2). They also inserted a film array between fabrics and obtained a sound-emitting flag (Figure 8h). This demonstrates the unique advantages of ferroelectret films as lightweight and flexible speakers. For micro-

phones, they compared the spectrograms of an original piece of music and the music recorded using a cellular PP ferroelectret microphone (Figure 8d,f,g). They confirmed its feasibility as a flexible microphone and demonstrated its first-rate recognition capabilities for computer user authentication (Figure 8e).

Several researchers have also achieved favorable results using ferroelectret films based on ePTFE, cross-linked PP or other materials in acoustic devices.[211–214] Yousry et al.[215] observed that PE ferroelectret films can reduce sound transmission by ≈30% compared to noncharged cellular films as soundproofing material, especially at sound frequencies exceeding 3000 Hz. They attributed this better performance to the charged cavities in the ferroelectret film, which convert a portion of sound waves into thermal energy (Figure 8i).

5.2. Wearable Health and Motion Monitors

For applications about wearable technology, Wu et al.[125] applied a cellular PP ferroelectret film as wearable sensor for detecting human biological signals (**Figure 9a**), such as coughing and pulse rate (Figure 9b); however, its application in wearable devices was limited, because of a relatively low piezoelectric coefficient and operating temperature. Sandwich-structured ferroelectret films produced by laser processing and 3D printing show high flexibility, low density, excellent biocompatibility, and exceptionally high piezoelectric coefficients. These quality features make them more suitable for wearable skin-contact sensors. Han et al.[157] built a wearable medical monitoring system using artificially perforated FEP films. It enabled them to collect vital information from the cardiovascular and respiratory systems in real time. Their device attained a signal-to-noise ratio comparable to that of medical recorders (BIOPAC) in detecting respiratory signals from the lung/tracheal region (Figure 9c).

Chu et al.[216] invoked artificially perforated ferroelectrets, with FEP and Ecoflex, made through hot pressing, as sensor to measure pulse waves at the Cun, Guan, and Chi points based on Traditional Chinese Medicine principles for medical assessments (Figure 9d). They assessed their accuracy and stability experimentally. Dali et al.[217] created PLA-based ferroelectret films using a similar approach. These devices, when attached to the forearm, can detect various gestures through monitoring the changes in electric signals (Figure 9e). They could identify specific gestures by using machine learning algorithms (Figure 9f). This eco-friendly and reliable solution opens up new possibilities for human–machine interaction.

Wan et al.[145] explored the use of ferroelectrets in bioelectronics. In order to obtain an implantable ferroelectret, they inserted a PVB film with parallel-connected air hole arrays between two FEP films with opposite charges, then coated these with gold electrodes. Next, they wrapped up the films, which are held together by electrostatic attraction, with medical-grade waterproof polyurethane and finally covered the whole structure with biocompatible PDMS (Figure 9g). They implanted the ferroelectret device in mice subcutaneously (Figure 9h,i) and showed that the activity of surrounding cells decreased somewhat over time (Figure 9j). Xiang et al.[218] developed a novel threadlike

ADVANCED
SCIENCE NEWS

www.advancedsciencenews.com

ADVANCED
MATERIALS

www.advmat.de
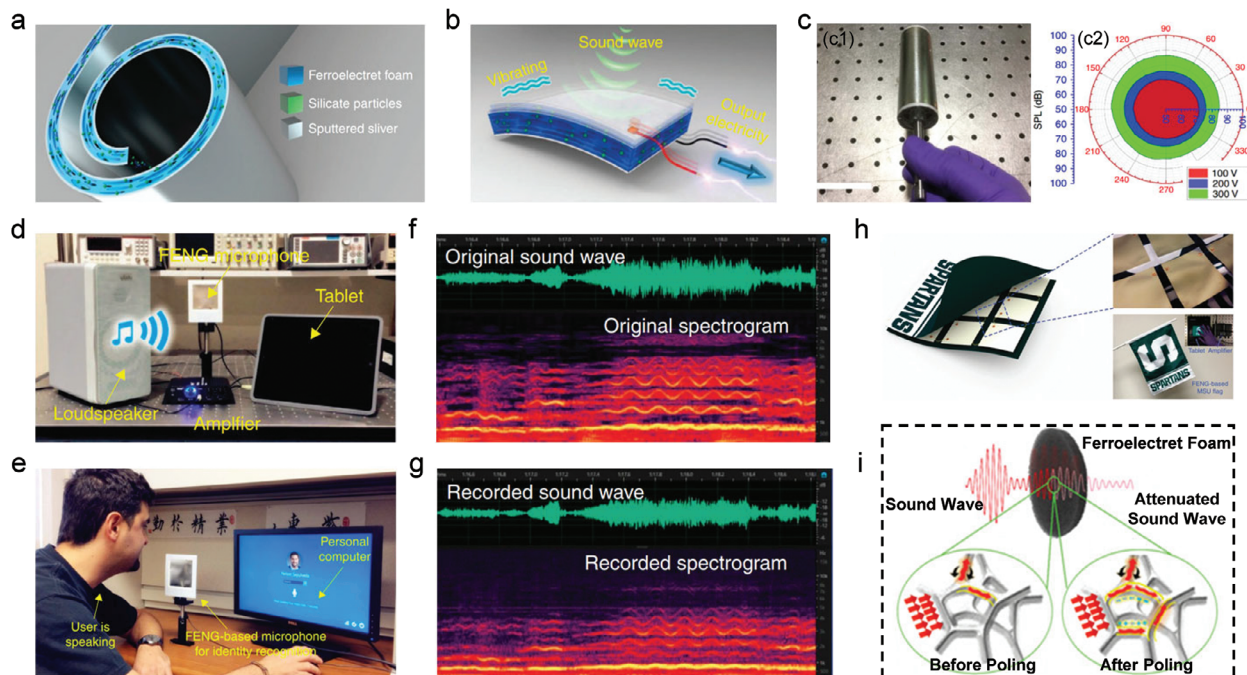
Figure 8. Applications of ferroelectret films in acoustic devices. a) Structure of the ferroelectret film used. b) Diagram of a ferroelectret-based microphone, and c) representation of the speaker and its sound pressure level (SPL) polar plots for different frequencies and voltages. d) Experimental setup for the FENG microphone and e) scenario for identity recognition. Comparison of f) original and g) recorded sound wave. h) Built-in array of ferroelectret films for a music-playing flag. a-h) Reproduced with permission.[202] Copyright 2016, Springer Nature. i) Picture of the sound insulation effect of ferroelectrets. Reproduced with permission.[215] Copyright 2022, MDPI.

piezoelectric pressure sensor based on IXPP, integrated it into textiles for the production of washable and breathable smart clothing, which could identify simple movements such as wrist flexion. Many researchers have explored the application of ferroelectret films for sensing in wearable devices for medical diagnostics and human–machine interaction.[219,220] Numerous experiments have indicated their practicality, diverse applicability, and enormous potential in various real-world scenarios.[221,222]

5.3. Noncontact Health Monitors

Shi et al.[206] developed a self-powered pressure sensor based on a low-density polyethylene (LDPE) ferroelectret (**Figure 10**a) for smart seats. The sensor relies on a 4-pixel sensor array and can monitor wirelessly the user's sitting posture in real time (Figure 10b). It thus offers a convenient, nonintrusive method for posture tracking. Ma et al.[223] designed a highly sensitive flexible pressure sensor with a folded structure based on IXPP (Figure 10c). This sensor could detect not only low-frequency human movements (Figure 10d), but also weak physiological signals without contact. This approach reduces interference and discomfort associated with prolonged wearing (Figure 10e–h).

Another monitor is a sleep monitoring device called EMFIT QS (Quantified Sleep). It consists of a thin ferroelectret sensor placed under the bed mattress. The device can estimate sleep patterns, analyses sleep quality, and tracks heart and respiratory rates during sleep. Ranta et al.[224] compared the data from this device with professional medical equipment and confirmed the accuracy of its data acquisition.

5.4. Energy Harvester

Ferroelectret films can generate real-time electrical signals with a high energy conversion efficiency. This makes them suitable for FENG applications that harvest mechanical energy from the environment to power electronic devices. Luo et al.[225] used a multilayered PP ferroelectret film as FENG to power a Zigbee transmitter (**Figure 11**a). They showed that the FENG placed under a person's insole could transmit 8-bit data using the energy harvested from every three to four steps. They also investigated the energy harvesting capabilities of ferroelectret films with different numbers of layers (Figure 11b). Li et al.[100] developed a lightweight, highly flexible and foldable film-based FENG using cellular PP film (Figure 11c). They found that folding improves its energy harvesting capability and enables self-powered keyboards and LCD screens (Figure 11d,e). The LCD screen could display preset patterns by collecting energy from user touches. Cao et al.[226] designed a fully integrated power management system that could efficiently harness the mechanical energy converted by their FENG to power LCD screens (Figure 11f,g). Zhong et al.[207] presented a PP-based FENG that can power a wireless transmitter by harvesting the mechanical energy generated from human walking. They also tested its self-recovery ability after exposure to extreme humid conditions.

5.5. Other Applications

Moreover, researchers discovered that PP ferroelectret can sense negative pressure and fabricated a sensitive waterproof ferroelec-

**ADVANCED
SCIENCE NEWS**

www.advancedsciencenews.com

**ADVANCED
MATERIALS**

www.advmat.de
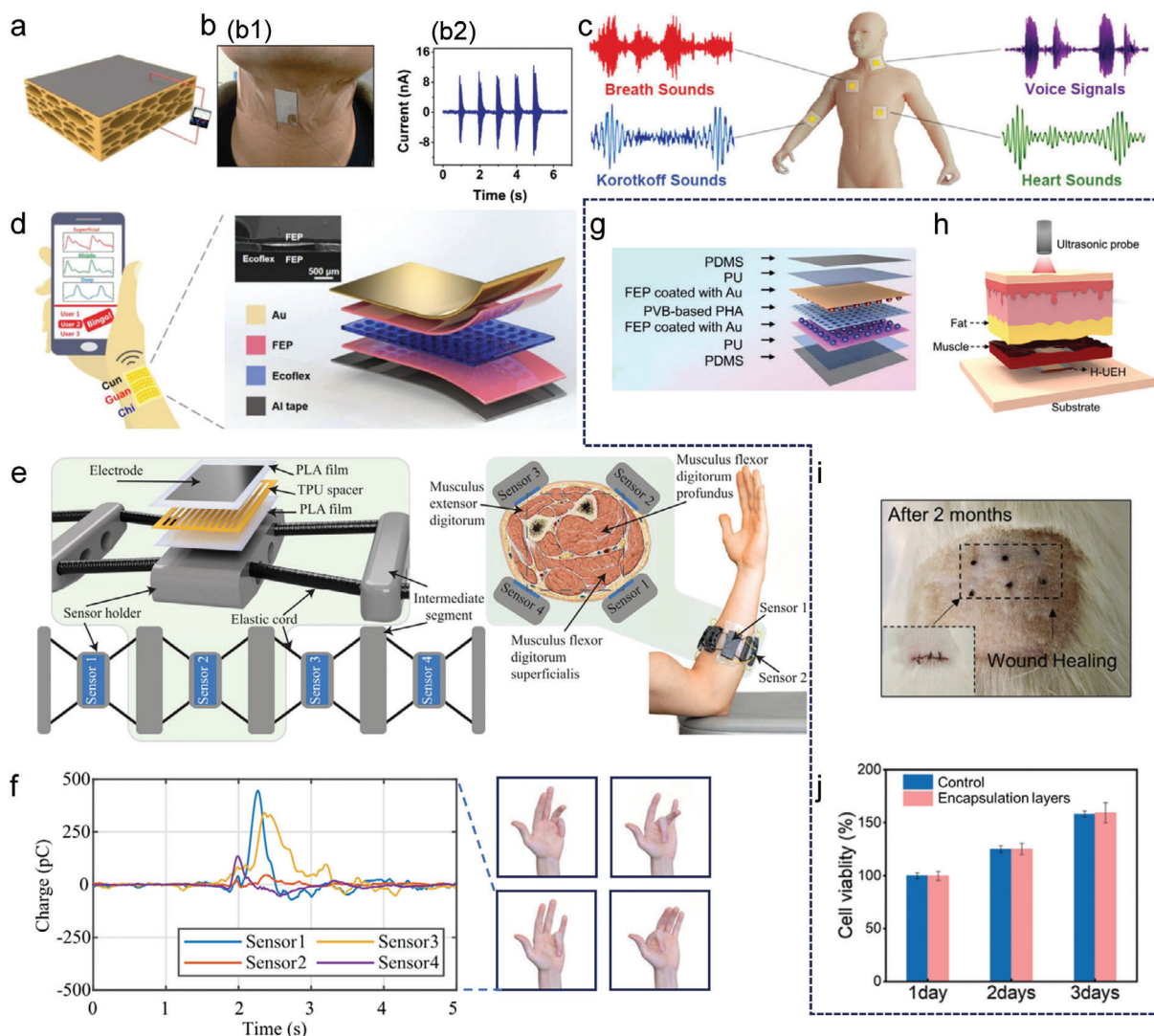
Figure 9. Highly sensitive ferroelectret films for wearable applications. a) Diagram of PP ferroelectret film. b) A PP ferroelectret sensor for monitoring human coughing. b1) Optical image of the sensing system. b2) Monitored coughing sounds through changes in electrical current. a,b) Reproduced with permission.[125] Copyright 2015, Wiley-VCH GmbH & Co. KGaA. c) Monitoring effects of the FEP-based ferroelectret sensors at different positions on the body. Reproduced with permission.[157] Copyright 2023, Wiley-VCH GmbH. d) Structure of the FEP-based ferroelectret film and representation of its application for monitoring pulse waves at Cun, Guan, and Chi positions. Reproduced with permission.[216] Copyright 2018, Wiley-VCH GmbH & Co. KGaA. e) Array sensors made from a sandwich ferroelectret film based on PLA, and f) its use for gesture recognition, with the palm initially fully open. Reproduced with permission.[217] Copyright 2023, IEEE. g) Exploded view of the FEP-based FENG for implantable bioelectronics. h) Side view of an energy harvester implanted into porcine fat and muscle, designed for generating ultrasound energy to initiate electrical stimulation. i) Optical image of the healing process two months after implantation in mice. j) Comparison of cell viability in a glass culture dish after a certain time. g-j) Reproduced with permission.[145] Copyright 2022, Wiley-VCH GmbH.

tret sensor for in situ monitoring lamprey spawning migration in natural underwater environments.[43,44] Open-cavity ferroelectret films are potentially vulnerable to charge loss in humid environments. They have not yet been examined for underwater monitoring tasks. Sealing around the edges using hot pressing may enable use of open-cavity ferroelectrets in wet conditions.

6. Conclusions and Outlook

Ferroelectrets generate electrical energy when their macrodipole moment changes under the action of a mechanical force.

They have garnered widespread attention due to their superior piezoelectric behavior and advantages such as high flexibility and low mass density. This review classifies ferroelectret films according to their cavity structure and fabrication route, provides an overview of three typical d_{33} models, analyzes the mechanisms and methods for improving the piezoelectric performance and explores various applications of ferroelectrets in human life. Moreover, the future advancement of ferroelectrets regarding preparation, performance optimization, and growth in applications was also discussed.

**ADVANCED
SCIENCE NEWS**

www.advancedsciencenews.com

**ADVANCED
MATERIALS**

www.advmat.de
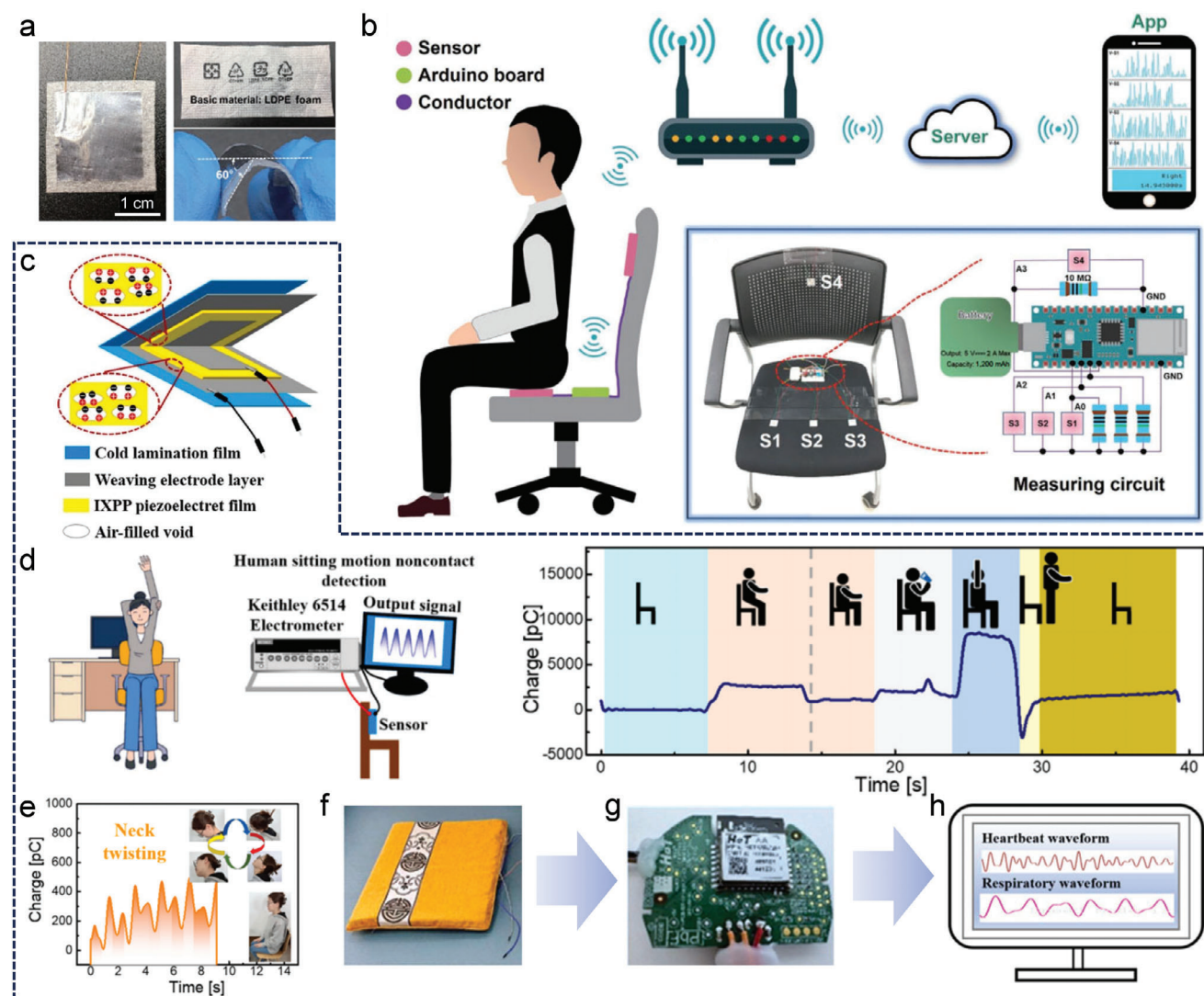
Figure 10. Application of ferroelectrets in noncontact health monitors. a) Optical image of a ferroelectret film sensor based on LDPE, demonstrating its flexibility through bending. b) Application in a smart chair, enabling real-time tracking of user's sitting positions. a, b) Reproduced with permission.[206] Copyright 2022, Tsinghua University Press. c) Exploded view of a ferroelectret sensor based on IXPP, d) its application in a smart cushion and its real-time electrical response for various sitting positions, and e) its application for identifying human neck movements. Optical image of f) smart cushion and g) data processing circuit board. h) Image of a real-time monitoring interface. c-h) Reproduced with permission.[223] Copyright 2023, Elsevier Ltd.

1) Porous polymer ferroelectret films primarily fall in two categories closed and open-cavity structures. Following contact charging or corona charging, DBDs ionize the air inside the cavities. This leads to the formation of stable macroscopic dipoles, which pop up in both bipolar and unipolar ferroelectrets. In closed-cavities ferroelectrets, the bipolar charges are trapped at the internal surfaces of cavities, whereas in the open-cavities ferroelectrets they reside for a large part at the porous/solid interface, for instance, between the open porous PTFE and solid FEP films.

2) The manufacturing of films with closed cavities involves stretching and foaming. Subsequent steps including gas expansion, uniaxial stretching, and short-term hot-press treatment are drawn in for optimizing the cavity structure. Ferroelectret films with open cavities are produced by hot pressing a porous PTFE film and two solid FEP films to sandwich structures. To improve the designability of cavity structures, artificial processing methods including mechanical machining, laser processing and 3D printing have emerged rapidly in recent years. Films with purposely designed regular cavity structures often exhibit exceptionally high d_{33} coefficients after charging.

The choice of manufacturing method of ferroelectrets should be guided by considering the melting points of the polymers, requirements for cavity structure and the desired piezoelectric performance. Physical foaming works well for materials with a low melting point, while hot pressing of a multilayer sandwich is suitable for high-temperature-resistant material with open porous structure. Mechanical machining and laser processing are convenient for creating
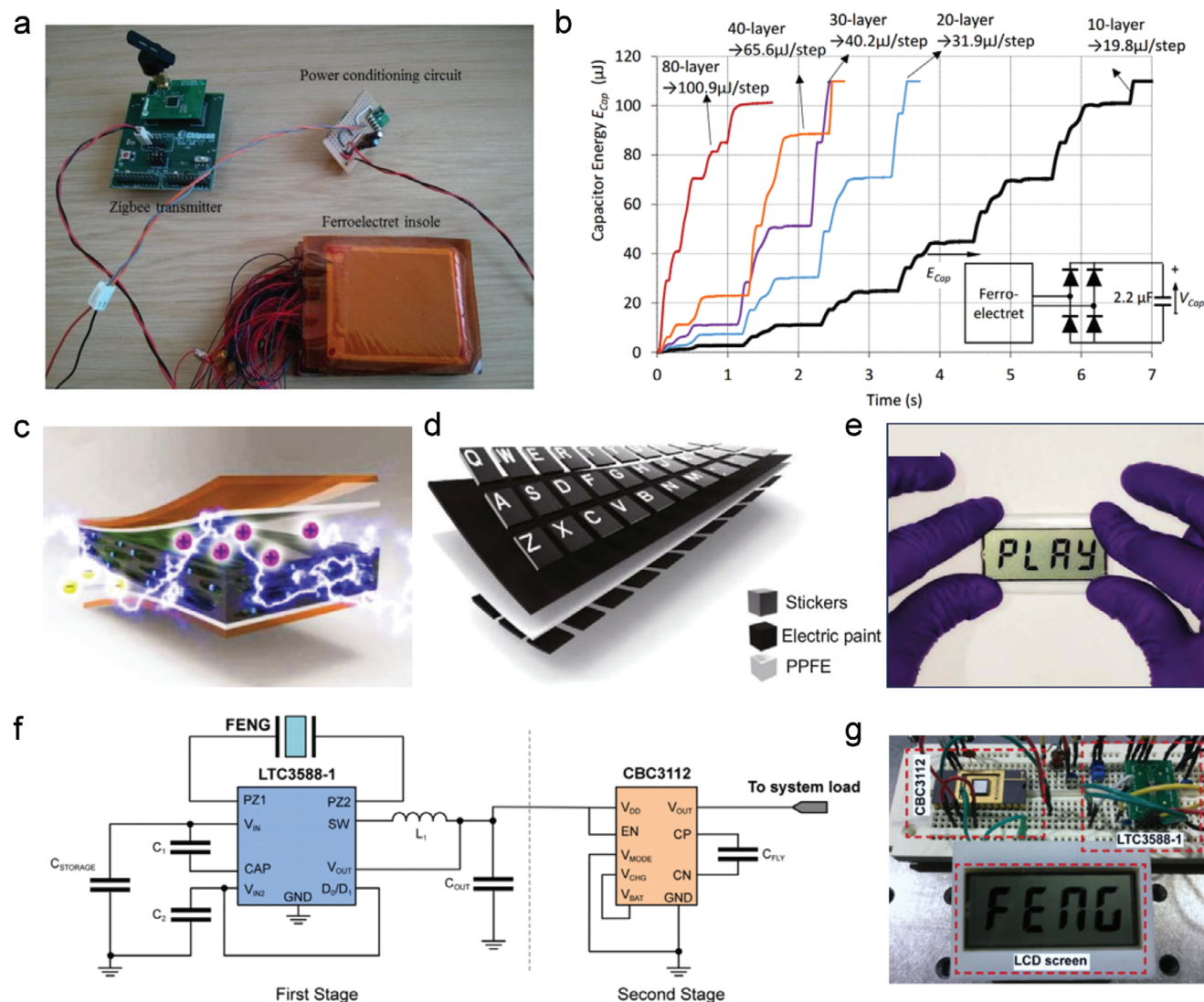
Figure 11. Application of ferroelectret films in energy harvesting. a) Optical image of a multilayered PP FENG serving as a power source for Zigbee transmitter. b) Charging curves of a 2.2 μF capacitor charged by PP ferroelectrets composed of different numbers of layers. a,b) Reproduced with permission.[225] Copyright 2015, IOP Publishing Ltd. c) Diagram of a FENG based on PP. d) Picture of the self-powered keyboard. e) Optical image of a self-powered LCD, which collects energy from finger pressure to display patterns. c-e) Reproduced with permission.[100] Copyright 2016, Elsevier Ltd. f) Circuit of an energy harvesting system and g) optical image of an LCD display powered by this energy harvester. f,g) Reproduced with permission.[226] Copyright 2019, American Chemical Society.

simple tubular cavities. 3D printing on the other hand offers ease of manufacturing and exceptional piezoelectric sensitivity. It holds great promise for the fabrication of regular cavity structures. Expanding the range of printable materials and advancing new precision printing would allow a precise adjustment of the cavities and the Young's modulus of dipole phases, thereby extending the number of applications.

3) Three modeling methods are reviewed that establish the relation between the structural characteristics of ferroelectrets and their piezoelectric properties. Several approaches for enhancing the piezoelectricity are also elucidated, including optimizing the design of cavity structures, replacing metal electrodes by fabric electrodes, injecting additional ions, using of

DC bias voltage and the synergy of foam structure and ferroelectric effect. These enhancement strategies also confirm the validity of the models.

The cavity geometries can be optimized through several approaches. These include controlling the foaming process to fine-tune pore structures, designing laminated structures for open-cavity ferroelectrets, improving precision in laser processing, and developing higher-precision 3D printing. Expanding the range of materials capable of producing open-cavity structures would facilitate the application of ion-boosting methods. The implementation of fabric electrodes and the application of DC bias voltage hold promise for further enhancing the piezoelectric performance of ferroelectrets.

4) Ferroelectret films have been applied in diverse fields, such as acoustical devices, health monitors, low-frequency piezoelectric sensing, and energy harvesting. It is underlined that the performance of ferroelectret-based acoustic devices is comparable to that of conventional microphones and speakers. Ferroelectret films used in wearable devices mostly feature regular cavity structures with high sensitivity. They offer high precision information for human–machine interaction and accurate real-time medical monitoring. Ferroelectrets applied in low-frequency piezoelectric sensing in smart seats and energy harvester for driving low-power devices, usually have a higher Young's modulus and piezoelectric coefficient.

Apart from one application for monitoring sleep under the mattress produced commercially by EMFIT, ferroelectrets are mainly applied in laboratory settings. To broaden the scope, a higher sensitivity and enhanced biocompatibility are essential. Challenges imposed by harsh environmental conditions like high temperature and humidity can be tackled using materials with higher heat resistance or structures that ensure charge stability.

As wearable electronics become more prevalent, enhancing the piezoelectric response of ferroelectrets, and optimizing the cavity structures for specific applications will become increasingly urgent. Mass production and standardization of ferroelectret films, enabling custom-made piezoelectric and mechanical performance also look promising. In the near future, we can anticipate the integration of ferroelectrets into wearable intelligent systems, which will facilitate their commercialization on a large scale.

## Conflict of Interest

The authors declare no conflict of interest.

[1] H. C. Ates, P. Q. Nguyen, L. Gonzalez-Macia, E. Morales-Narváz, F. Guder, J. J. Collins, C. Dincer, *Nat. Rev. Mater.* **2022**, *7*, 887.

[2] E. Hittinger, P. Jaramillo, *Science* **2019**, *364*, 326.

[3] L. Portilla, K. Loganathan, H. Faber, A. Eid, J. G. D. Hester, M. M. Tentzeris, M. Fattori, E. Cantatore, C. Jiang, A. Nathan, G. Fiori, T. Ibn-Mohammed, T. D. Anthopoulos, V. Pecunia, *Nat. Electron.* **2023**, *6*, 10.

[4] S. R. A. Ruth, L. Beker, H. Tran, V. R. Feig, N. Matsuhisa, Z. A. Bao, *Adv. Funct. Mater.* **2020**, *30*, 1903100.

[5] J. C. Yang, J. Mun, S. Y. Kwon, S. Park, Z. N. Bao, S. Park, *Adv. Mater.* **2019**, *31*, 1904765.

[6] X. Li, B. Qi, X. Wan, J. Zhang, W. Yang, Y. Xiao, F. Mao, K. Cai, L. Huang, J. Zhou, *Nano Energy* **2023**, *114*, 108652.

[7] M. Mardonova, Y. Choi, *Energies* **2018**, *11*, 547.

[8] A. Kamisalic, I. Fister, M. Turkanovic, S. Karakatic, *Sensors* **2018**, *18*, 1714.

[9] G. R. Chen, X. Xiao, X. Zhao, T. Tat, M. Bick, J. Chen, *Chem. Rev.* **2022**, *122*, 3259.

[10] D. W. Fu, H. L. Cai, Y. M. Liu, Q. Ye, W. Zhang, Y. Zhang, X. Y. Chen, G. Giovannetti, M. Capone, J. Y. Li, R. G. Xiong, *Science* **2013**, *339*, 425.

[11] S. Park, S. W. Heo, W. Lee, D. Inoue, Z. Jiang, K. Yu, H. Jinno, D. Hashizume, M. Sekino, T. Yokota, K. Fukuda, K. Tajima, T. Someya, *Nature* **2018**, *561*, 516.

[12] Q. S. Yang, T. Wei, R. T. Yin, M. Z. Wu, Y. M. Xu, J. Koo, Y. S. Choi, Z. Q. Xie, S. W. Chen, I. Kandela, S. L. Yao, Y. J. Deng, R. Avila, T. L. Liu, W. B. Bai, Y. Y. Yang, M. D. Han, Q. H. Zhang, C. R. Haney, K. B. Lee, K. Aras, T. Wang, M. H. Seo, H. W. Luan, S. M. Lee, A. Brikha, N. Ghoreishi-Haack, L. Tran, I. Stepien, F. Aird, et al., *Nat. Mater.* **2021**, *20*, 1559.

[13] C. Bowen, H. Kim, P. Weaver, S. J. E. Dunn, *Energy Environ. Sci.* **2014**, *7*, 25.

[14] T. Karaki, K. Yan, M. Adachi, *Jpn. J. Appl. Phys.* **2007**, *46*, 7035.

[15] J.-F. Li, K. Wang, F.-Y. Zhu, L.-Q. Cheng, F.-Z. Yao, *J. Am. Ceram. Soc.* **2013**, *96*, 3677.

[16] P. Li, J. Zhai, B. Shen, S. Zhang, X. Li, F. Zhu, X. Zhang, *Adv. Mater.* **2018**, *30*, 1705171.

[17] W.-Q. Liao, D. Zhao, Y.-Y. Tang, Y. Zhang, P.-F. Li, P.-P. Shi, X.-G. Chen, Y.-M. You, R.-G. Xiong, *Science* **2019**, *363*, 1206.

[18] M. Habib, I. Lantgios, K. Hornbostel, *J. Phys. D: Appl. Phys.* **2022**, *55*, 423002.

[19] S. Trolier-McKinstry, S. Zhang, A. J. Bell, X. Tan, *Annu. Rev. Mater. Res.* **2018**, *48*, 191.

[20] L.-Q. Cheng, J.-F. Li, *J. Mater.* **2016**, *2*, 25.

[21] L. J. Gibson, M. F. Ashby, *Cellular Solids: Structure and Properties*, Cambridge University Press, New York **1999**.

[22] J. Hao, W. Li, J. Zhai, H. Chen, *Mater. Sci. Eng., R* **2019**, *135*, 1.

[23] S. Bauer, R. Gerhard(-Multhaupt), G. M. Sessler, *Phys. Today* **2004**, *57*, 37.

[24] K. N. Kim, J. Chun, S. A. Chae, C. W. Ahn, I. W. Kim, S.-W. Kim, Z. L. Wang, J. M. Baik, *Nano Energy* **2015**, *14*, 87.

[25] A. Almusallam, Z. Luo, A. Komolafe, K. Yang, A. Robinson, R. Torah, S. Beeby, *Nano Energy* **2017**, *33*, 146.

[26] H. Gong, Y. Zhang, J. Ye, X. Zhou, X. Zhou, Y. Zhao, K. Feng, H. Luo, D. Zhang, C. Bowen, *Adv. Funct. Mater.* **2024**, *34*, 2311091.

[27] Q. Xu, Z. Wang, J. Zhong, M. Yan, S. Zhao, J. Gong, K. Feng, J. Zhang, K. Zhou, J. Xie, H. Xie, D. Zhang, Y. Zhang, C. Bowen, *Adv. Funct. Mater.* **2023**, *33*, 2304402.

[28] A. A. Tezcan, C. R. Bowen, G. Poulin-Vittrant, H. Khanbareh, J. I. Roscow, *2023 IEEE Int. Symp. on Applications of Ferroelectrics (ISAF)*, IEEE, New York **2023**.

[29] H. Kawai, *Jpn. J. Appl. Phys.* **1969**, *8*, 975.

[30] L. Lu, W. Ding, J. Liu, B. Yang, *Nano Energy* **2020**, *78*, 105251.

[31] X. Chen, X. Han, Q.-D. Shen, *Adv. Electron. Mater.* **2017**, *3*, 1600460.

[32] W. Xia, Z. Zhang, *IET Nanodielectr.* **2018**, *1*, 17.

[33] B. Stadlober, M. Zirkl, M. Irimia-Vladu, *Chem. Soc. Rev.* **2019**, *48*, 1787.

[34] M. Smith, S. Kar-Narayan, *Int. Mater. Rev.* **2022**, *67*, 65.

[35] S. Mohammadpourfazeli, S. Arash, A. Ansari, S. Yang, K. Mallick, R. Bagherzadeh, *RSC Adv.* **2023**, *13*, 370.

[36] *Electromechanically Active Polymers. A Concise Reference*, (Ed: F. Carpi), Springer, Berlin **2016**.

**ADVANCED
SCIENCE NEWS**

www.advancedsciencenews.com

**ADVANCED
MATERIALS**

www.advmat.de

[37] K. Kirjavainen, US Patent 4 654 546, **1987**.

[38] A. Savolainen, K. Kirjavainen, *J. Macromol. Sci. A* **1989**, *26*, 583.

[39] S. Bauer, *IEEE Trans. Dielectr. Electr. Insul.* **2006**, *13*, 953.

[40] M. Lindner, S. Bauer-Gogonea, S. Bauer, M. Paajanen, J. Raukola, *J. Appl. Phys.* **2002**, *91*, 5283.

[41] X. Qiu, R. Gerhard, A. Mellinger, *IEEE Trans. Dielectr. Electr. Insul.* **2011**, *18*, 34.

[42] V. N. Kestelman, L. S. Pinchuk, V. A. Goldade, *Electrets in Engineering: Fundamentals and Applications*, Springer Science & Business Media, Berlin **2000**.

[43] Y. Cao, H. Shi, X. Tan, N. Sepulveda, *IEEE Sens. Lett.* **2022**, *6*, 1.

[44] Y. Cao, H. Shi, X. Tan, N. Sepúlveda, *Nano Res.* **2022**, *16*, 11822.

[45] A. Mellinger, M. Wegener, W. Wirges, R. R. Mallepally, R. Gerhard(-Multhaupt), *Ferroelectrics* **2006**, *331*, 189.

[46] O. Hamdi, F. Mighri, D. Rodrigue, *Polym. Adv. Technol.* **2018**, *30*, 153.

[47] G. O. Braña, P. L. Segovia, F. Magraner, A. Quijano, *J. Phys.: Conf. Ser.* **2011**, *301*, 012054.

[48] Z. Ruan, Q. Hu, M. Zhang, W. Liu, G. Zhu, M. Chen, X. Zhang, *Appl. Phys. Lett.* **2023**, *122*, 242904.

[49] J. Zhong, Q. Zhong, X. Zang, N. Wu, W. Li, Y. Chu, L. Lin, *Nano Energy* **2017**, *37*, 268.

[50] P. Fang, M. Wegener, W. Wirges, R. Gerhard, L. Zirkel, *Appl. Phys. Lett.* **2007**, *90*, 192908.

[51] P. Fang, X. Qiu, W. Wirges, R. Gerhard, L. Zirkel, *IEEE Trans. Dielectr. Electr. Insul.* **2010**, *17*, 1079.

[52] Z. Xia, J. Jiang, Y. Zhang, Y. Cao, Z. Wang, in *Annual Report, IEEE Conf. on Electrical Insulation and Dielectric Phenomena (CEIDP)*, Vol. *2*, IEEE, New York **1997**, p. 471.

[53] Z. Hu, H. von Seggern, *J. Appl. Phys.* **2006**, *99*, 024102.

[54] Y. Cao, Z. Xia, Q. Li, J. Shen, L. Chen, B. Zhou, *IEEE Trans. Dielectr. Electr. Insul.* **1998**, *5*, 58.

[55] O. Voronina, M. Wegener, W. Wirges, R. Gerhard, L. Zirkel, H. Münstedt, *Appl. Phys. A* **2007**, *90*, 615.

[56] X. Ma, H. von Seggern, G. M. Sessler, S. Zhukov, O. B. Dali, M. Kupnik, X. Zhang, *Smart Mater. Struct.* **2021**, *30*, 015002.

[57] S. Zhukov, X. Ma, H. von Seggern, G. M. Sessler, O. B. Dali, M. Kupnik, X. Zhang, *Appl. Phys. Lett.* **2020**, *117*, 112901.

[58] D. Vadas, K. Bocz, T. Igricz, J. Volk, S. Bordács, L. Madarász, G. Marosi, *Adv. Ind. Eng. Polym. Res.* **2023**, *7*, 215.

[59] E. Saarimäki, M. Paajanen, A. Savijarvi, H. Minkkinen, M. Wegener, O. Voronina, R. Schulze, W. Wirges, R. Gerhard(-Multhaupt), *IEEE Trans. Dielectr. Electr. Insul.* **2006**, *13*, 963.

[60] H. Wang, X. Wang, M. Wadsworth, M. F. Ahmed, Z. Liu, C. Zeng, *Micromachines* **2022**, *13*, 1177.

[61] R. Kacprzyk, E. Motyl, in *8th Int. Symp. on Electrets (ISE 8)*, IEEE, New York **1994**, p. 703.

[62] R. Kacprzyk, E. Motyl, J. B. Gajewski, A. Pasternak, *J. Electrostat.* **1995**, *35*, 161.

[63] R. Kacprzyk, A. Dobrucki, J. B. Gajewski, *J. Electrostat.* **1997**, *39*, 33.

[64] N. Wang, R. Daniels, L. Connelly, M. Sotzing, C. Wu, R. Gerhard, G. A. Sotzing, Y. Cao, *Small* **2021**, *17*, 2103161.

[65] P. Fang, F. Wang, W. Wirges, R. Gerhard, H. C. Basso, *Appl. Phys. A* **2011**, *103*, 455.

[66] P. C. Sherrell, A. Šutka, M. Timusk, A. Šutka, *Small* **2024**, 2311570.

[67] J. X. Zhu, Y. X. Yang, H. Zhang, Z. J. Zhao, T. Hu, L. Liu, *Adv. Funct. Mater.* **2023**, *33*, 2214859.

[68] L. Wang, M. Hu, K. Kong, J. Tao, K. Ji, Z. Dai, *Nano Energy* **2022**, *104*, 107934.

[69] Y. Zhang, C. R. Bowen, S. K. Ghosh, D. Mandal, H. Khanbareh, M. Arafa, C. Y. Wan, *Nano Energy* **2019**, *57*, 118.

[70] X. Mo, H. Zhou, W. Li, Z. Xu, J. Duan, L. Huang, B. Hu, J. Zhou, *Nano Energy* **2019**, *65*, 104033.

[71] X. Zhang, H. von Seggern, G. M. Sessler, M. Kupnik, *IEEE Electr. Insul. Mag.* **2020**, *36*, 47.

[72] Z. Y. Li, Y. Cui, J. W. Zhong, *Biosens. Bioelectron.* **2021**, *186*, 113290.

[73] M. A. Ansari, P. Somdee, *Adv. Energy Sustainability Res.* **2022**, *3*, 2200063.

[74] X. Qiu, in *Electromechanically Active Polymers. A Concise Reference*, 1st ed. (Ed: F. Carpi), Polymers and Polymeric Composites Series, Springer, Berlin **2016**, p. 561.

[75] X. Qiu, Y. Bian, J. Liu, Y. Xiang, T. Ding, W. Zhu, F.-Z. Xuan, *IET Nanodielectr.* **2022**, *5*, 113.

[76] X. Qiu, P. Fang, A. Mellinger, R. A. P. Altafim, W. Wirges, G. Gidion, D. Rychkov, *J. Adv. Dielectr.* **2023**, *13*, 2341009.

[77] W. Li, Y. Cao, C. Wang, N. Sepulveda, *Cell Rep. Phys. Sci.* **2023**, *4*, 101388.

[78] X. Zhang, J. Zhao, P. Xie, S. Wang, *J. Funct. Biomater.* **2023**, *14*, 320.

[79] H. Ohigashi, *J. Appl. Phys.* **2008**, *47*, 949.

[80] S. Zhukov, S. Fedosov, H. von Seggern, *J. Phys. D: Appl. Phys.* **2011**, *44*, 105501.

[81] M. Wegener, W. Wirges, R. Gerhard-Multhaupt, *Adv. Eng. Mater.* **2005**, *7*, 1128.

[82] B. Notario, J. Pinto, M. A. Rodríguez-Pérez, *Polymer* **2015**, *63*, 116.

[83] X. Qiu, A. Mellinger, M. Wegener, W. Wirges, R. Gerhard, *J. Appl. Phys.* **2007**, *101*, 104112.

[84] X. Qiu, L. Holländer, W. Wirges, R. Gerhard, H. Cury Basso, *J. Appl. Phys.* **2013**, *113*, 224106.

[85] R. Hippler, S. Pfau, M. Schmidt, K. H. Schoenbach, *Low Temperature Plasma Physics: Fundamental Aspects and Applications*, Wiley-VCH, Weinheim, Germany **2001**.

[86] S. Harris, A. Mellinger, *Appl. Phys. A* **2012**, *107*, 553.

[87] S. Harris, O. Mellinger, A. Mellinger, *Annual Report, IEEE Conf. on Electrical Insulation and Dielectric Phenomena (CEIDP)*, IEEE, New York **2010**, p. 1. DOI: 10.1109/CEIDP.2010.5723939

[88] Z. Hu, H. von Seggern, *J. Appl. Phys.* **2005**, *98*, 014108.

[89] S. Zhukov, H. von Seggern, *J. Appl. Phys.* **2007**, *101*, 084106.

[90] S. Zhukov, H. von Seggern, in *2010 10th IEEE Int. Conf. on Solid Dielectrics*, IEEE, New York **2010**, p. 1. DOI: 10.1109/ICSD.2010.5568127

[91] N. Wang, J. van Turnhout, R. Daniels, C. Wu, J. Huo, R. Gerhard, G. Sotzing, Y. Cao, *ACS Appl. Mater. Interfaces* **2022**, *14*, 42705.

[92] P. Zhang, Z. Xia, X. Qiu, F. Wang, X. Wu, in *2005 12th Int. Symp. on Electrets*, IEEE, New York **2005**, p. 39.

[93] D. Rychkov, W. Wirges, R. Gerhard, R. A. P. Altafim, in *Annual Report, IEEE Conf. on Electrical Insulation and Dielectric Phenomena (CEIDP)*, IEEE, New York **2015**, p. 84.

[94] X. Ma, X. Zhang, in *2018 IEEE 2nd Int. Conf. on Dielectrics (ICD)*, IEEE, New York **2018**, p. 1. DOI: 10.1109/ICD.2018.8514773

[95] X. Zhang, G. M. Sessler, X. Ma, Y. Xue, L. Wu, *J. Micromech. Microeng.* **2018**, *28*, 065012.

[96] X. Ma, X. Zhang, G. M. Sessler, L. Chen, X. Yang, X. Dai, P. He, *AIP Adv.* **2019**, *9*, 125334.

[97] D. Rychkov, A. Rychkov, N. Efimov, A. Malygin, R. Gerhard, *Appl. Phys. A* **2013**, *112*, 283.

[98] R. Gerhard(-Multhaupt), *IEEE Trans. Dielectr. Electr. Insul.* **2002**, *9*, 850.

[99] Z. Xia, A. Wedel, R. Danz, *IEEE Trans. Dielectr. Electr. Insul.* **2003**, *10*, 102.

[100] W. Li, D. Torres, T. Y. Wang, C. Wang, N. Sepulveda, *Nano Energy* **2016**, *30*, 649.

[101] S. Mishra, L. Unnikrishnan, S. K. Nayak, S. Mohanty, *Macromol. Mater. Eng.* **2019**, *304*, 1800463.

[102] O. B. Dali, H. von Seggern, G. M. Sessler, P. Pondrom, S. Zhukov, X. Zhang, M. J. N. S. Kupnik, *Nano Sci.* **2022**, *3*, 713.

[103] X. Zhang, P. Pondrom, G. M. Sessler, X. Ma, *Nano Energy* **2018**, *50*, 52.

[104] H. von Seggern, S. Zhukov, S. Fedosov, *IEEE Trans. Dielectr. Electr. Insul.* **2011**, *18*, 49.

[105] N. Wang, K. Davis, M. Sotzing, M. A. Baferani, J. Huo, C. B. Carter, R. Gerhard, Y. Cao, in *IEEE Conf. on Electrical Insulation and Dielectric Phenomena (CEIDP)*, IEEE, New York **2021**, p. 375.

[106] M. Paajanen, J. Lekkala, K. Kirjavainen, *Sens. Actuators, A* **2000**, *84*, 95.

[107] A. Mohebbi, F. Mighri, A. Ajji, D. Rodrigue, *Adv. Polym. Tech.* **2016**, *37*, 468.

[108] R. A. Shammeh, Ph.D. Thesis, The University of Western Ontario (Canada) **2019**.

[109] S. P. Nalawade, F. Picchioni, L. P. B. M. Janssen, *Prog. Polym. Sci.* **2006**, *31*, 19.

[110] A. Mohebbi, F. Mighri, A. Ajji, D. Rodrigue, *J. Appl. Polym. Sci.* **2016**, *134*, 44577.

[111] S. Nagō, S. Nakamura, Y. Mizutani, *J. Appl. Polym. Sci.* **1992**, *45*, 1527.

[112] J. Raukola, *A New Technology to Manufacture Polypropylene Foam Sheet and Biaxially Oriented Foam Film*, VTT Technical Research Centre of Finland, Espoo, FI **1998**.

[113] H. Gilbert-Tremblay, F. Mighri, D. Rodrigue, *J. Cell. Plast.* **2012**, *48*, 341.

[114] N. Behrendt, V. Altstadt, H.-W. Schmidt, X. Zhang, G. M. Sessler, *IEEE Trans. Dielectr. Electr. Insul.* **2006**, *13*, 992.

[115] N. Behrendt, *IEEE Trans. Dielectr. Electr. Insul.* **2010**, *17*, 1113.

[116] M. Paajanen, H. Minkkinen, J. Raukola, in *Proc. of the 11th Int. Symp. on Electrets*, IEEE, New York **2002**, p. 191.

[117] M. Wegener, W. Wirges, J. Fohlmeister, B. Tiersch, R. Gerhard(-Multhaupt), *J. Phys. D: Appl. Phys.* **2004**, *37*, 623.

[118] X. Zhang, J. Hillenbrand, G. M. Sessler, *Appl. Phys. Lett.* **2004**, *85*, 1226.

[119] A. I. Cooper, *Adv. Mater.* **2003**, *15*, 1049.

[120] A. Mohebbi, F. Mighri, A. Ajji, D. Rodrigue, *Cell. Polym.* **2017**, *36*, 13.

[121] W. Wirges, M. Wegener, O. Voronina, L. Zirkel, R. Gerhard(-Multhaupt), *Adv. Funct. Mater.* **2007**, *17*, 324.

[122] X. Ma, S. Zhukov, H. von Seggern, G. M. Sessler, O. B. Dali, M. Kupnik, Y. Dai, P. He, X. Zhang, *Adv. Electron. Mater.* **2023**, *9*, 2201070.

[123] X. Zhang, J. Huang, J. Chen, Z. Wan, S. Wang, Z. Xia, *Appl. Phys. Lett.* **2007**, *91*, 182901.

[124] X. Zhang, L. Wu, G. M. Sessler, *AIP Adv.* **2015**, *5*, 077185.

[125] N. Wu, X. Cheng, Q. Zhong, J. Zhong, W. Li, B. Wang, B. Hu, J. Zhou, *Adv. Funct. Mater.* **2015**, *25*, 4788.

[126] H. von Seggern, *J. Appl. Phys.* **1979**, *50*, 7039.

[127] M. Wegener, W. Wirges, B. Tiersch, *J. Porous Mater.* **2007**, *14*, 111.

[128] A. Mellinger, M. Wegener, W. Wirges, R. Gerhard(-Multhaupt), *Appl. Phys. Lett.* **2001**, *79*, 1852.

[129] R. Schwodiauer, G. S. Neugschwandtner, K. Schrattbauer, M. Lindner, M. Vieytes, S. Bauer-Gogonea, S. Bauer, *IEEE Trans. Dielectr. Electr. Insul.* **2000**, *7*, 578.

[130] R. L. Remke, H. von Seggern, *J. Appl. Phys.* **1983**, *54*, 5262.

[131] R. Gerhard(-Multhaupt), *IEEE Trans. Electr. Insul.* **1987**, *EI-22*, 531.

[132] Z. Xia, R. Gerhard(-Multhaupt), W. Künstler, A. Wedel, R. Danz, *J. Phys. D: Appl. Phys.* **1999**, *32*, L83.

[133] X. Zhang, J. Huang, Z. Xia, *Phys. Scr.* **2007**, *T129*, 274.

[134] J. Huang, X. Zhang, Z. Xia, X. Wang, *J. Appl. Phys.* **2008**, *103*, 084111.

[135] B. Wang, J. Zhong, Q. Zhong, N. Wu, X. Cheng, W. Li, K. Liu, L. Huang, B. Hu, J. Zhou, *Adv. Electron. Mater.* **2016**, *2*, 1500408.

[136] B. Wang, C. Liu, Y. Xiao, J. Zhong, W. Li, Y. Cheng, B. Hu, L. Huang, J. Zhou, *Nano Energy* **2017**, *32*, 42.

[137] J. Shi, S. Yong, S. Beeby, *Smart Mater. Struct.* **2018**, *27*, 084005.

[138] J. Shi, S. P. Beeby, *Smart Mater. Struct.* **2022**, *31*, 045015.

[139] Y. Zhang, C. R. Bowen, S. Deville, *Soft Matter* **2019**, *15*, 825.

[140] J.-J. Wang, T.-H. Hsu, C.-N. Yeh, J.-W. Tsai, Y.-C. Su, *J. Micromech. Microeng.* **2012**, *22*, 015013.

[141] G. M. Sessler, G. M. Yang, W. Hatke, in *Annual Report, IEEE Conf. on Electrical Insulation and Dielectric Phenomena (CEIDP)*, Vol. 2, IEEE, New York **1997**, p. 467.

[142] G. M. Yang, G. M. Sessler, W. Hatke, in *Proc. of the 10th Int. Symp. on Electrets (ISE 10) (Cat. No. 99 CH36256)*, IEEE, New York **1999**, p. 317.

[143] R. A. C. Altafim, H. C. Basso, R. A. P. Altafim, L. Lima, C. V. d. Aquino, L. G. Neto, R. Gerhard(-Multhaupt), *IEEE Trans. Dielectr. Electr. Insul.* **2006**, *13*, 979.

[144] R. A. P. Altafim, X. Qiu, W. Wirges, R. Gerhard, R. A. C. Altafim, H. C. Basso, W. Jenninger, J. Wagner, *J. Appl. Phys.* **2009**, *106*, 014106.

[145] X. Wan, P. Chen, Z. Xu, X. Mo, H. Jin, W. Yang, S. Wang, J. Duan, B. Hu, Z. Luo, L. Huang, J. Zhou, *Adv. Funct. Mater.* **2022**, *32*, 2200589.

[146] X. Ma, C. Song, F. Zhang, Y. Dai, P. He, X. Zhang, *ACS Appl. Mater. Interfaces* **2022**, *14*, 51291.

[147] X. Ma, X. Chen, X. Xiang, F. Zhang, Y. Zhao, F. Wang, X. Mu, Y. Dai, P. He, X. Zhang, *Nano Energy* **2022**, *103*, 107729.

[148] S. Zhukov, D. Eder-Goy, S. Fedosov, B. X. Xu, H. von Seggern, *Sci. Rep.* **2018**, *8*, 4597.

[149] Z. Xu, X. Wan, X. Mo, S. Lin, S. Chen, J. Chen, Y. Pan, H. Zhang, H. Jin, J. Duan, L. Huang, L.-B. Huang, J. Xie, F. Yi, B. Hu, J. Zhou, *Nano Energy* **2021**, *89*, 106450.

[150] X. Huiming, C. Gangjin, C. Xumin, C. Zhi, *Sci. Rep.* **2017**, *7*, 8443.

[151] G. J. Chen, M. F. Lei, H. M. Xiao, L. Wu, *Chin. Phys. Lett.* **2014**, *31*, 127702.

[152] W. Lai, Q. Lou, J. Zhang, Z. Fan, Q. Wang, C. H. Park, G. Chen, *Nano Energy* **2022**, *95*, 107057.

[153] H. C. Basso, R. A. P. Altafim, R. A. C. Altafim, A. Mellinger, P. Fang, W. Wirges, R. Gerhard, in *Annual Report, IEEE Conf. on Electrical Insulation and Dielectric Phenomena (CEIDP)*, IEEE, New York **2007**, p. 453.

[154] Y. Li, C. Zeng, *Macromol. Chem. Phys.* **2013**, *214*, 2733.

[155] L. Han, W. Zeng, Y. Dong, X. Wang, L. Lin, *Adv. Electron. Mater.* **2022**, *8*, 2200012.

[156] J.-J. Wang, J.-W. Tsai, Y.-C. Su, *J. Micromech. Microeng.* **2013**, *23*, 075009.

[157] L. Han, W. Liang, Q. Xie, J. Zhao, Y. Dong, X. Wang, L. Lin, *Adv. Sci.* **2023**, *10*, 2301180.

[158] G. Taormina, C. Sciancalepore, M. Messori, F. Bondioli, *J. Appl. Biomater. Funct. Mater.* **2018**, *16*, 151.

[159] M. Sborikas, X. Qiu, W. Wirges, R. Gerhard, W. Jenninger, D. Lovera, *Appl. Phys. A* **2014**, *114*, 515.

[160] I. Kierzewski, S. S. Bedair, B. Hanrahan, H. Tsang, L. B. Hu, N. Lazarus, *Addit. Manuf.* **2020**, *31*, 100963.

[161] A. Mirkowska, R. Kacprzyk, K. Rozmaryniewicz, *IEEE Trans. Dielectr. Electr. Insul.* **2022**, *29*, 823.

[162] O. B. Dali, S. Zhukov, M. Rutsch, C. Hartmann, H. von Seggern, G. M. Sessler, M. Kupnik, *IEEE Int. Ultrason. Symp.* **2021**, https://doi.org/10.1109/IUS52206.2021.9593738.

[163] H. von Seggern, S. Zhukov, O. B. Dali, C. Hartmann, G. M. Sessler, M. Kupnik, *Polymers* **2021**, *13*, 3751.

[164] Y. A. O. Assagra, R. A. P. Altafim, J. P. do Carmo, R. A. C. Altafim, D. Rychkov, W. Wirges, R. Gerhard, *IEEE Trans. Dielectr. Electr. Insul.* **2020**, *27*, 1668.

[165] D. Saini, A. Kumar, H. K. Mishra, V. Gupta, B. Mondal, Z. Mallick, D. Mandal, *Sens. Actuators, A* **2023**, *365*, 114858.

[166] G. Perna, F. Bonacci, S. Caponi, A. Clementi, A. Di Michele, L. Gammaitoni, M. Mattarelli, I. Neri, D. Puglia, F. Cottone, *Nanomaterials* **2023**, *13*, 2953.

[167] A. Kumar, D. Saini, D. Mandal, *Appl. Phys. Lett.* **2022**, *120*, 182901.

[168] K. Tao, H. Yi, Y. Yang, H. Chang, J. Wu, L. Tang, Z. Yang, N. Wang, L. Hu, Y. Fu, *Nano Energy* **2020**, *67*, 104197.

[169] Z. Zhai, L. Wu, H. Jiang, *Appl. Phys. Rev.* **2021**, *8*, 041319.

[170] G. M. Sessler, J. Hillenbrand, in *10th Int. Symp. on Electrets (ISE 10)*, IEEE, New York **1999**, p. 261.

[171] J. Hillenbrand, G. M. Sessler, *IEEE Trans. Dielectr. Electr. Insul.* **2000**, *7*, 537.

[172] M. Paajanen, H. Valimaki, J. Lekkala, in *10th Int. Symp. on Electrets (ISE 10)*, IEEE, New York **1999**, p. 735.

[173] M. Paajanen, J. Lekkala, H. Valimaki, *IEEE Trans. Dielectr. Electr. Insul.* **2001**, *8*, 629.

[174] R. Gerhard, in *Annual Report, IEEE Conf. on Electrical Insulation and Dielectric Phenomena (CEIDP)*, IEEE, New York **2014**, p. 1, https://doi.org/10.1109/CEIDP.2014.6995800.

[175] N. Wang, M. A. Baferani, R. Daniels, C. Wu, J. Huo, J. van Turnhout, G. A. Sotzing, R. Gerhard, Y. Cao, *J. Phys. D: Appl. Phys.* **2024**, *57*, 145502.

[176] R. Gerhard, S. Bauer, X. Qiu, in *IEEE Conf. on Electrical Insulation and Dielectric Phenomena (CEIDP)*, IEEE, New York **2016**, p. 81.

[177] R. Gerhard, presented at IEEE 19th Internat. Symp. on Electrets (ISE-19), Linz, Austria, September, 2023.

[178] J. I. Roscow, Y. Zhang, M. J. Kraśny, R. W. C. Lewis, J. Taylor, C. R. Bowen, *J. Phys. D: Appl. Phys.* **2018**, *51*, 225301.

[179] S. Harris, A. Mellinger, *J. Appl. Phys.* **2014**, *115*, 163302.

[180] M. Wegener, W. Wirges, R. Gerhard(-Multhaupt), M. Dansachmüller, R. Schwödiauer, S. Bauer-Gogonea, S. Bauer, M. Paajanen, H. Minkkinen, J. Raukola, *Appl. Phys. Lett.* **2004**, *84*, 392.

[181] Y. Feng, K. Hagiwara, Y. Iguchi, Y. Suzuki, *Appl. Phys. Lett.* **2012**, *100*, 262901.

[182] Y. Feng, Y. Suzuki, in *2013 IEEE 26th Int. Conf. on Micro Electro Mechanical Systems (MEMS)*, IEEE, New York **2013**, p. 865.

[183] H. Cury Basso, J. R. B. d. A. Monteiro, D. Baladelli Mazulquim, G. Teixeira de Paula, L. Gonçalves Neto, R. Gerhard, *J. Appl. Phys.* **2013**, *114*, 104101.

[184] Z. Wang, G. Chen, X. Hong, J. Yu, J. Zhang, Y. Ding, Q. Lou, H. He, *J. Electrost.* **2022**, *116*, 103683.

[185] Z. Pan, G. Liu, X. Chen, A. A. Babar, X. Dong, X. Wang, *J. Text. Inst.* **2022**, *113*, 2128.

[186] J. van Turnhout, S. T. Abrahami, in *19th Int. Symp. on Electrets (ISE 19)*, IEEE, New York **2023**, p. 92.

[187] L. Zhang, M. Fairbanks, T. L. Andrew, *Adv. Funct. Mater.* **2017**, *27*, 1700415.

[188] X. Qiu, R. Gerhard, A. Mellinger, *IEEE Trans. Dielectr. Electr. Insul.* **2010**, *17*, 1043.

[189] J. Hillenbrand, G. M. Sessler, *J. Appl. Phys.* **2008**, *103*, 074103.

[190] J. Döring, V. Bovtun, J. Bartusch, A. Erhard, M. Kreutzbruck, Y. Yakymenko, *Appl. Phys. A* **2010**, *100*, 479.

[191] J. Döring, V. Bovtun, M. Gaal, J. Bartusch, A. Erhard, M. Kreutzbruck, Y. Yakymenko, *J. Appl. Phys.* **2012**, *112*, 084505.

[192] V. Bovtun, J. Döring, J. Bartusch, M. Gaal, A. Erhard, M. Kreutzbruck, Y. Yakymenko, *Adv. Appl. Ceram.* **2013**, *112*, 97.

[193] M. Gaal, R. Caldeira, J. Bartusch, F. Schadow, K. Vössing, M. Kupnik, *IEEE Trans. Ultrason. Ferroelectr. Freq. Control* **2019**, *66*, 1600.

[194] K. Roy, S. Jana, S. K. Ghosh, B. Mahanty, Z. Mallick, S. Sarkar, C. Sinha, D. Mandal, *Langmuir* **2020**, *36*, 11477.

[195] S. K. Ghosh, T. K. Sinha, B. Mahanty, S. Jana, D. Mandal, *J. Appl. Phys.* **2016**, *120*, 174501.

[196] C. Xu, L. Jin, L. Zhang, C. Wang, X. Huang, X. He, Y. Xu, R. Huang, C. Zhang, W. Yang, J. Lu, *Compos. Sci. Technol.* **2018**, *164*, 282.

[197] C. Xu, L. Zhang, Y. Xu, Z. Yin, Q. Chen, S. Ma, H. Zhang, R. Huang, C. Zhang, L. Jin, *J. Mater. Chem. A* **2017**, *5*, 189.

[198] T. Kaura, V. K. Srivastava, *J. Electrostat.* **1987**, *19*, 45.

[199] W. Eisenmenger, H. Schmidt, B. Dehlen, *Braz. J. Phys.* **1999**, *29*, 295.

[200] T. T. C. Palitó, Y. A. O. Assagra, R. A. P. Altafim, J. P. Carmo, R. A. C. Altafim, *Measurement* **2019**, *131*, 42.

[201] H. Dsouza, A. Van Schyndel, J. Pastrana, Y. Cao, E. Hunter, B. Rakerd, N. Sepúlveda, *J. Sound Vib.* **2020**, *468*, 115091.

[202] W. Li, D. Torres, R. Diaz, Z. Wang, C. Wu, C. Wang, Z. Lin Wang, N. Sepulveda, *Nat. Commun.* **2017**, *8*, 15310.

[203] J. Nie, M. Ji, Y. Chu, X. Meng, Y. Wang, J. Zhong, L. Lin, *Nano Energy* **2019**, *58*, 528.

[204] K. Ichikawa, W. Hijikata, *Nano Energy* **2022**, *99*, 107357.

[205] Y. Cao, J. Figueroa, W. Li, Z. Chen, Z. L. Wang, N. Sepúlveda, *Nano Energy* **2019**, *63*, 103852.

[206] Y. Shi, K. Zhang, S. Ding, Z. Li, Y. Huang, Y. Pi, D. Zhao, Y. Zhang, R. Wang, B. Zhou, Z.-X. Yang, J. Zhong, *Nano Res.* **2022**, *16*, 1269.

[207] J. Zhong, Q. Zhong, G. Chen, B. Hu, S. Zhao, X. Li, N. Wu, W. Li, H. Yu, J. Zhou, *Energy Environ. Sci.* **2016**, *9*, 3085.

[208] H. Holzmann, Y. J. Park, G. Stoll, H. Atzrodt, S. Herold, *Smart Mater. Struct.* **2023**, *32*, 125013.

[209] J. Hillenbrand, G. M. Sessler, *J. Acoust. Soc. Am.* **2004**, *116*, 3267.

[210] J. Hillenbrand, G. M. Sessler, *IEEE Trans. Dielectr. Electr. Insul.* **2006**, *13*, 973.

[211] M. Ploner, N. Wang, C. Wu, R. Daniels, J. Huo, G. A. Sotzing, Y. Cao, *iScience* **2022**, *25*, 105607.

[212] C. Song, X. Ma, J. Zhao, J. Zhang, F. Yang, Y. Pan, X. Zhang, *IEEE Trans. Dielectr. Electr. Insul.* **2022**, *29*, 777.

[213] Z. Song, X. Cai, Y. Wang, W. Yang, W. Li, *Micromachines* **2023**, *14*, 2145.

[214] D. Yang, L. Zhang, L. Wang, K. Wang, *ACS Appl. Electron. Mater.* **2023**, *5*, 6063.

[215] Y. M. Yousry, E. C. Statharas, K. Yao, A. M. Mohamed, P. C. Lim, F. E. H. Tay, *Polymers* **2022**, *14*, 4843.

[216] Y. Chu, J. Zhong, H. Liu, Y. Ma, N. Liu, Y. Song, J. Liang, Z. Shao, Y. Sun, Y. Dong, X. Wang, L. Lin, *Adv. Funct. Mater.* **2018**, *28*, 1803413.

[217] O. B. Dali, S. Zhukov, R. Chadda, A. Kasanski, H. von Seggern, X. Zhang, G. M. Sessler, M. Kupnik, *IEEE Sens. J.* **2023**, *23*, 1943.

[218] X. Xiang, X. Ma, L. Zhou, G. M. Sessler, H. von Seggern, O. B. Dali, M. Kupnik, P. He, Y. Dai, X. Zhang, *Adv. Mater. Technol.* **2023**, *8*, 2202130.

[219] X. Ma, Q. Hu, Y. Dai, P. He, X. Zhang, *Sens. Actuators, A* **2022**, *346*, 113834.

[220] P. Fang, X. Ma, X. Li, X. Qiu, R. Gerhard, X. Zhang, G. Li, *IEEE Sens. J.* **2018**, *18*, 401.

[221] H. Dsouza, J. Pastrana, J. Figueroa, I. Gonzalez-Afanador, B. M. Davila-Montero, N. Sepulveda, *Sci. Rep.* **2022**, *12*, 8567.

[222] O. B. Dali, Y. Sellami, S. Zhukov, H. von Seggern, N. Schafer, B. Latsch, G. M. Sessler, P. Beckerle, M. Kupnik, *IEEE Sens.* **2022**, https://doi.org/10.1109/SENSORS52175.2022.9967198.

[223] X. Ma, Y. Qi, Y. Niu, Q. Zhang, X. Xiang, K. Zhang, P. He, Y. Dai, W. Niu, X. Zhang, *Nano Energy* **2023**, *111*, 108424.

[224] J. Ranta, T. Aittokoski, M. Tenhunen, M. Alasaukko-oja, *Biomed. Phys. Eng. Express* **2019**, *5*, 025016.

[225] Z. Luo, D. Zhu, S. P. Beeby, *J. Phys.: Conf. Ser.* **2015**, *660*, 012118.

[226] Y. Cao, J. Figueroa, J. J. Pastrana, W. Li, Z. Chen, Z. L. Wang, N. Sepulveda, *ACS Appl. Mater. Interfaces* **2019**, *11*, 17400.
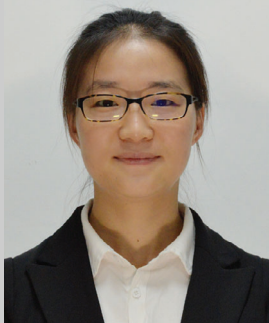
Ningzhen Wang is an associate professor at School of Technology of Beijing Forestry University. She obtained her Bachelor's degree from Huazhong University of Science and Technology, and Ph.D. from Tsinghua University, then she engaged in postdoctoral research at Technische Universität Berlin and University of Connecticut. Her research focuses on porous materials including ferroelectrets and metal foams. She enhanced the piezoelectric performance of expanded PTFE-based ferroelectrets by optimizing their stacking structure, cavity size, using fabric electrodes and prefilling additional ions. She is interested in developing novel fabrication methods and elucidating the piezoelectric mechanisms of high-performance ferroelectrets.

Xunlin Qiu received the Ph.D. from Tongji University in 2006. From 2006 to 2020, he worked in teaching and research at the University of Potsdam and the Technical University of Chemnitz in Germany. In 2017, he obtained the highest German university degree, the Habilitation (Dr. rer. nat. habil.) from the University of Potsdam. Since 2020, he has become a professor at East China University of Science and Technology in Shanghai, China. His research interest is functional dielectrics and electrets, and piezoelectricity in polar polymer films and nonpolar polymer foams and its applications.

Reimund Gerhard was born in Heidelberg. He studied mathematics and physics at TU Darmstadt and obtained a Dr.-Ing. degree in 1984. Dr. Gerhard was project manager at HHI Berlin 1985–1994 and appointed university professor of applied condensed-matter physics at U Potsdam in 1994. From 2008 to 2012, he was dean of the Faculty of Science. In 1993 and 2012, he was elected Fellow of IEEE and APS, respectively. 2018–2019, he served as President of the IEEE Dielectrics and Electrical Insulation Society. Research appointments took him to universities in Brazil, Canada, China, France, Germany, Israel, and the USA.

Jan van Turnhout obtained a degree in Applied Physics from the University of Technology Delft and a PhD degree from the University of Leyden. He worked at the Dutch Research Organisation TNO, where he led a Group on Electrical Properties of Polymers. Later became Head of the Dept. of Polymer Physics. His TNO-research was focused on developing electrets for microphones and electret filters. From 1989 to 2007 he was professor of Polymer Physics at the TU-Delft. At present he is emeritus at the Dept. Materials Science and Technology, where he studies the disinfection of seeds with corona discharges.

**ADVANCED
SCIENCE NEWS**

www.advancedsciencenews.com

**ADVANCED
MATERIALS**

www.advmat.de

Yang Cao is a full professor at the Electrical and Computer Engineering Department of the University of Connecticut, where he also serves as the Director of the Electrical Insulation Research Center, Institute of Materials Science and the Site Director of the NSF iUCRC Center on High Voltage/Temperature Materials and Structures. His research interests are in the physics of materials under extreme field and harsh conditions and the development of new dielectric materials and electroactive device for energy efficient power conversion and renewables integrations, as well as for novel medical diagnostic imaging.